

A ChIP-exo screen of 887 PCR⁺ transcription factor antibodies in human cells

William K. M. Lai^{1,2}, Luca Mariani³, Gerson Rothschild⁵, Edwin R. Smith⁶, Bryan J. Venters⁷, Thomas R. Blanda¹, Prashant K. Kuntala¹, Kylie Bocklund¹, Joshua Mairose¹, Sarah N Dweikat¹, Katelyn Mistretta¹, Matthew J. Rossi¹, Daniela James¹, James T. Anderson³, Sabrina K. Phanor³, Wanwei Zhang⁵, Zibo Zhao⁶, Avani P. Shah⁶, Katherine Novitzky⁷, Eileen McAnarney⁷, Michael-C. Keogh^{7*}, Ali Shilatifard^{6*}, Uttiya Basu^{5*}, Martha L. Bulyk^{3,4*}, B. Franklin Pugh^{1,2*}

¹Center for Eukaryotic Gene Regulation, Department of Biochemistry and Molecular Biology, The Pennsylvania State University, University Park, Pennsylvania 16802, USA

²Department of Molecular Biology and Genetics, Cornell University, Ithaca, NY 14853

³Division of Genetics, Department of Medicine; Brigham and Women's Hospital and Harvard Medical School, Boston, MA 02115.

⁴Department of Pathology; Brigham and Women's Hospital and Harvard Medical School, Boston, MA 02115.

⁵Department of Microbiology and Immunology, Vagelos College of Physicians and Surgeons, Columbia University, New York.

⁶Simpson Querrey Center for Epigenetics and the Department of Biochemistry and Molecular Genetics, Northwestern University Feinberg School of Medicine, 303 East Superior Street, Chicago, IL 60611, USA

⁷EpiCypher Inc., Durham NC 27709

*Co-corresponding authors

Contact Information:

William KM Lai <wkl29@cornell.edu>

Luca Mariani <lucamariani77@gmail.com>

Gerson Rothschild <ger2@cumc.columbia.edu>

Edwin R. Smith <edwsmith@northwestern.edu>

Bryan J. Venters <bventers@epicypher.com>

Thomas R Blanda <trb5344@psu.edu>

Prashant K Kuntala <pxk284@psu.edu>

Kylie Bocklund <kxb357@psu.edu>

Joshua Mairose <josh.mairose@gmail.com>

Sarah N Dweikat <szd41@psu.edu>

Katelyn Mistretta <katelynmistretta@gmail.com>

Matthew J. Rossi <mjr26@psu.edu>

Daniela James <daniela.james@psu.edu>

41 James T. Anderson <jamesanderson12358@gmail.com>
42 Sabrina K. Phanor <sphanor@bwh.harvard.edu>
43 Wanwei Zhang <wz2370@cumc.columbia.edu>
44 Zibo Zhao <zibo.zhao@northwestern.edu>
45 Avani P. Shah <avani.shah1@northwestern.edu>
46 Katherine Novitzky <knovitzky@epicypher.com>
47 Eileen McAnarney <emcanarney@epicypher.com>
48 Michael-C. Keogh <mkeogh@epicypher.com>
49 Ali Shilatifard <ash@northwestern.edu>
50 Uttiya Basu <ub2121@cumc.columbia.edu>
51 Martha L. Bulyk <mlbulyk@genetics.med.harvard.edu>
52 B. Franklin Pugh <fp265@cornell.edu>
53

54 **Abstract**

55 Antibodies offer a powerful means to interrogate specific proteins in a complex milieu.
56 However, antibody availability and reliability are problematic and epitope tagging can be
57 impractical in many cases. In an effort to improve this situation, the Protein Capture Reagents
58 Program (PCRP) generated over a thousand renewable monoclonal antibodies (mAbs) against
59 human-presumptive chromatin proteins. However, these reagents have not been widely field-
60 tested. We therefore performed a screen to test their ability to enrich genomic regions via
61 chromatin immunoprecipitation (ChIP) and a variety of orthogonal assays. 887 unique antibodies
62 against 681 unique human transcription factors (TFs), were assayed by ultra-high resolution
63 ChIP-exo/seq, primarily in a single pass in one cell type (K562). Deep systematic analyses of the
64 resulting ~1,200 ChIP-exo datasets can be found at www.PCRPvalidation.org. Subsets of PCRP
65 mAbs were further tested in ChIP-seq, CUT&RUN, STORM super-resolution microscopy,
66 immunoblots, and protein binding microarray (PBM) experiments. About 5% of the tested
67 antibodies displayed target (i.e., cognate antigen) enrichment across at least one assay and are
68 strong candidates for additional validation. An additional 34% produced ChIP-exo data that was
69 distinct from background and thus warrant further testing. The remaining 61% were not
70 substantially different from background, and likely require consideration of a much broader
71 survey of cell types and/or assay optimizations. We demonstrate and discuss the metrics and
72 challenges to antibody validation in chromatin-based assays.

74 **Introduction**

75 Antibodies are a critical component of a wide variety of biochemical assays. They serve
76 as protein-specific affinity-capture and detection reagents, useful *in vivo* and *in vitro*. Example
77 assays include chromatin immunoprecipitation (ChIP) of protein-DNA interactions,
78 immunofluorescence, immunoblotting, ELISA, purification of cells and proteins, protein binding
79 microarray (PBM) experiments, and targeted *in vivo* delivery of effector molecules (Chames et
80 al. 2009; Park 2009; Siggers et al. 2011a; Mahmood and Yang 2012; Engelen et al. 2015; Lin et
81 al. 2015). One advantage of target-specific antibodies is their ability to recognize proteins
82 without the need for an engineered affinity tag. The human proteome contains tens of thousands
83 of distinct proteins, each requiring a different antibody for specific detection. The usage of a
84 variety of antibodies to diverse targets has been a critical component of NIH-funded consortium
85 projects such as the ENCODE and Roadmap Epigenomics Mapping (Consortium 2012;
86 Roadmap Epigenomics et al. 2015). However, broad profiling of the genomic targets of human
87 sequence-specific transcription factors (ssTFs) has been limited by the availability of ‘ChIP-
88 grade’ antibodies.

89 Overall, there has been an acute lack of antibodies that effectively distinguish the many
90 thousands of different chromatin proteins. Consistency in reagent production and performance
91 have been particularly problematic (Egelhofer et al. 2011; Baker 2015; Shah et al. 2018).
92 Polyclonal antibodies, being a mixed product of many antibody genes, have the advantage of
93 potentially recognizing multiple epitopes on a protein, thereby producing robust target detection
94 (Hanly et al. 1995). However, their production is finite, and can be variable across immunized

95 animals, but also vary within individuals by different bleed dates and affinity purifications.
96 These factors and more hamper reproducibility (Reardon 2016).

97 The NIH Protein Capture Reagent Program (PCRP) was initiated through the NIH
98 Common Fund with the stated goal of testing the feasibility of producing low-cost, renewable,
99 and reliable protein affinity reagents in a manner that can be scaled ultimately to the entire
100 human proteome (PA-16-287) (<https://proteincapture.org/>) (Blackshaw et al. 2016). With an
101 initial focus on putative ssTFs, this endeavor reported the production of 1,406 mouse monoclonal
102 antibodies (mAbs) against 737 chromatin protein targets (Venkataraman et al. 2018). This
103 included two parallel production approaches: mouse hybridomas that release mAb into growth
104 medium supernatant, and recombinant antibodies produced in *E. coli*. The advantages of these
105 two approaches over polyclonal antibodies are, in principle, a renewable and consistent supply of
106 homogeneous preparations produced from a single set of genes that recognize a single epitope
107 (Kohler and Milstein 1975; Winter et al. 1994; Liu 2014). To accommodate the potential
108 shortcoming of a hybridoma recognizing a single non-viable epitope, the NIH PCRP made an
109 effort to generate at least two independent clones for each target, although this does not
110 guarantee two different epitopes, as in cases where there are immunodominant regions.

111 Antibody validation is required to generate confidence in their utility (Baker 2015; Marx
112 2019). Validation exists at many levels ranging from whether an antibody specifically recognizes
113 its intended target to the exclusion of all others, to whether it consistently performs successfully
114 in a particular assay (Landt et al. 2012; Wardle and Tan 2015; Uhlen et al. 2016; Edfors et al.
115 2018; Sikorski et al. 2018). Each publicly available PCRP-generated antibody was previously
116 validated for its target recognition by *in vitro* human protein (HuProt) microarray screening
117 (Venkataraman et al. 2018). These arrays contain approximately equivalent amounts of antigen,
118 which differs from the wide expression range in natural sources. They also may differ in epitope
119 accessibility compared to complexed or crosslinked targets in ChIP assays. Thus, additional
120 assay-specific validation is necessary. The further capability of PCRP antibodies has been
121 described for a limited set in a number of approaches, including immunoblotting,
122 immunoprecipitation, immunohistochemistry, and ChIP-seq, with assay-dependent success
123 observed (Venkataraman et al. 2018). Previous work has reported that 46 of 305 mAbs against
124 36 of 176 targets passed ENCODE ChIP-seq standards (Venkataraman et al. 2018), although
125 detailed supporting evidence is not publicly available. “Browser shots” of selected loci from that
126 study are available for ~40 datasets against 31 targets. However, these should be considered
127 preliminary, since locus-specific examples lack statistical power and unbiased selection.
128 Additionally, chromatin fragmentation and extraction may generate localized variation in yield
129 that varies from prep to prep (active promoters, enhancers, etc.). Numerous replicates (target and
130 control) are often needed to ensure against false positives at selected individual loci due to
131 sampling variation and multiple hypothesis testing. As broader community use of the PCRP-
132 generated antibodies will likely benefit from a wider survey, we conducted additional tests of
133 these reagents. To our knowledge there has been no systematic large-scale field assessment of
134 antibodies in ChIP. We report on progress and challenges in comprehensively assaying ~1,400
135 PCRP mAbs. As this represents a first-pass assessment, most experiments include only a single
136 replicate, using enrichment of specific genomic features as preliminary evidence of success. We

137 performed replicates on some samples that displayed enrichment (e.g., expected motif
138 enrichment) as well as a subset of samples which displayed no initial enrichment to examine our
139 true negative rate.

140 Since evaluating each of ~1,400 mAbs in a wide variety of assays was not practical, we
141 opted for broad coverage by ChIP-exo, which we have developed into a high-throughput and
142 ultra-high resolution alternative to ChIP-seq (Rossi et al. 2018). ChIP-exo allows genome-wide
143 detection of chromatin interactions at near-bp resolution, which also increases the confidence of
144 peak calling. We further tested a smaller subset of mAbs in other assays (ChIP-seq, CUT&RUN,
145 super-resolution cellular microscopy (STORM), immunoblots, and protein binding microarrays).
146 These additional tests were not intended to be comprehensive, but rather to evaluate the
147 challenges and practicality of systematic antibody validation. Overall, we tested 946 unique mAb
148 clones (887 in ChIP-exo and 59 in other assays), of which 642 targeted putative ssTFs, which
149 allowed computational comparison through the enrichment of their cognate motifs (if one exists).
150 The antibodies and assays were chosen to cover a wide range of end-user applications, with
151 specific ssTFs chosen in part based on the scientific interests of the investigators and a set of
152 objective criteria. With a deep dive on a single assay (ChIP-exo), we explored end-user practical
153 issues related to antibody sourcing, reproducibility and validation metrics, and specificity for cell
154 types and states.

155

156 **Results**

157 **Screening PCRP mAb by ChIP-exo**

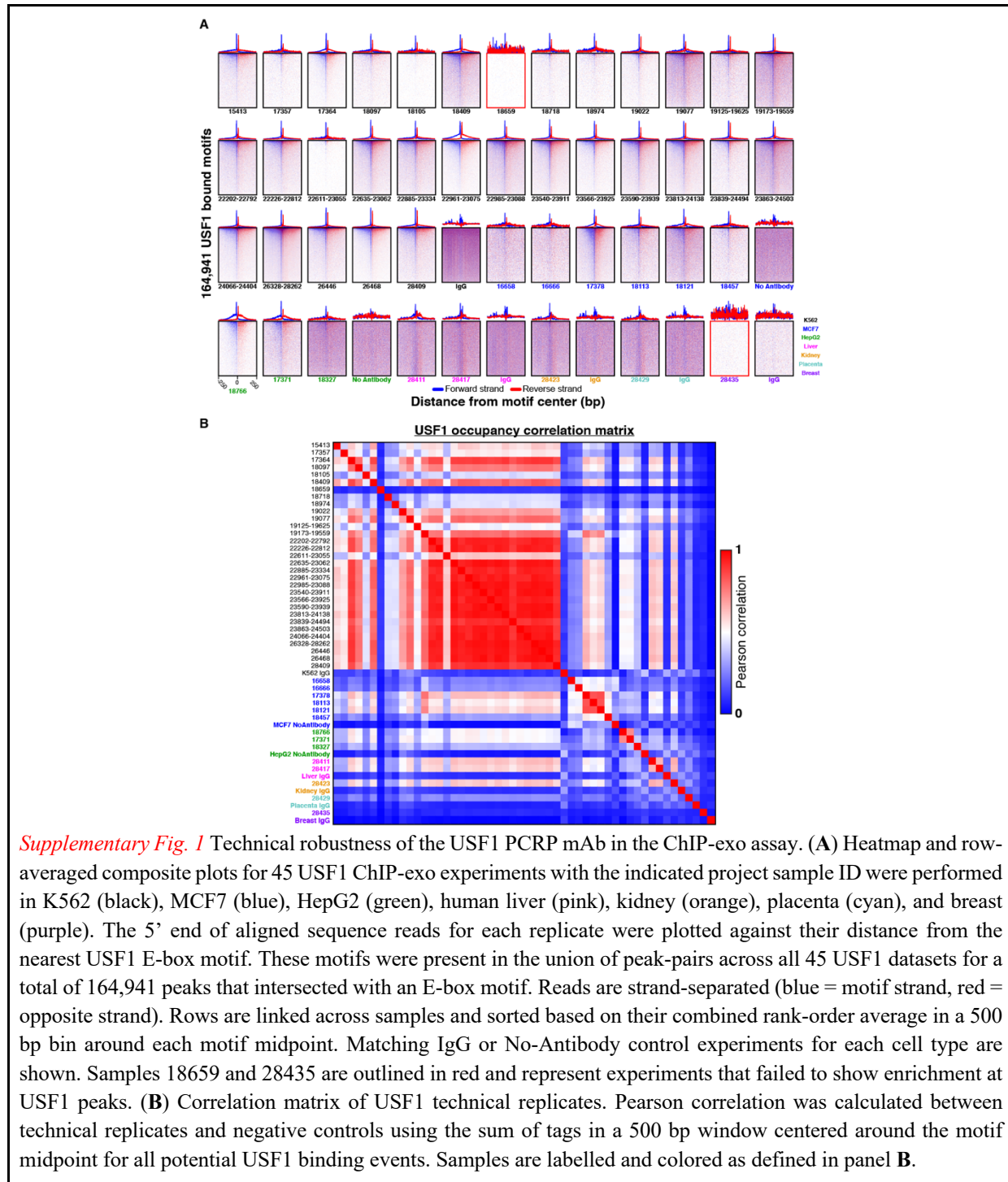
158 We used the massively parallel ChIP-exo version of ChIP-seq to screen PCRP Abs in 96-
159 well plate format (48 at a time) for their ability to recognize their putative protein targets in a
160 chromatinized, cellular context (Rhee and Pugh 2012; Rossi et al. 2018). Briefly, proteins were
161 formaldehyde crosslinked to DNA and each other within cells. Chromatin was then isolated,
162 fragmented, and immunoprecipitated. While on the beads, the fragmented DNA was trimmed
163 with a strand-specific 5'-3' exonuclease up to the point of crosslinking (i.e., protection), which
164 was then mapped by DNA sequencing. For many proteins, this provides single-bp resolution in
165 genome-wide detection (Rhee and Pugh 2011). Since ChIP-exo is a higher resolution derivative
166 of ChIP-seq, ChIP-exo is expected in principle to detect any real binding events that ChIP-seq
167 detects, and likely more due to its higher dynamic range.

168 Technical reproducibility of ChIP-exo with PCRP mAbs was evaluated with 43
169 independent replicates performed on the sequence-specific TF USF1. This replicate served as a
170 positive control in 43 cohorts, each having 46 mAb assayed on different days: as such no USF1
171 replicates were excluded in this analysis. We prioritized mAb evaluation in K562 (human bone
172 marrow lymphoblast), but also tested a subset in MCF7 (human mammary gland epithelial),
173 HepG2 (human liver, epithelial-like), and donated human tissues (liver, kidney, placenta, and
174 breast). From this and IgG (or no antibody) negative controls, we defined with USF1 a set of
175 ~164,000 E-box motif instances associated with a significant ($q < 0.01$) peak-pair in at least one
176 replicate ChIP-exo experiment (Albert et al. 2008). This reflects a very relaxed criterion, with a
177 high level of expected false positives, for the purposes of evaluating the gradient from true
178 binding through nonspecific background at genomic E-boxes. The latter is expected where a

179 peak location occurred in only a small fraction of datasets. When examined at greater stringency
180 regarding the number of replicates in which the same peak was found, a higher average
181 occupancy and more robust patterning was observed. Of the USF1 datasets, 43 of the 45 (>95%),
182 produced a USF1-specific ChIP-exo pattern around E-boxes (*Supplementary Fig. 1A*, vertical
183 blue and red stripes in the heat maps and single-bp peaks in the composite plots). A Pearson-
184 pairwise correlation was calculated for the occupancy of binding at putative USF1-bound E-
185 boxes across all USF1 and negative control IgG (or no antibody) ChIP datasets (*Supplementary*
186 *Fig. 1B*). A strong correlation among USF1 data sets was observed, which reflects a high level of
187 reproducibility and indicated that ChIP-exo was suitable for screening and evaluating PCR
188 mAbs in ChIP.

189 We initiated our ChIP mAb survey by first considering the practicality of producing a
190 large number of antibody preparations from *E. coli* or mouse hybridomas. Purification from *E.*
191 *coli* included transformation of expressing plasmids, cell growth, recombinant protein induction,
192 and purification. After multiple attempts, we determined that high throughput parallelized
193 recombinant immunoreagent production was not practical within the scope of this project, due to
194 a need to optimize the protocol in our hands. We therefore opted to pursue commercially
195 available hybridoma-based mAbs.

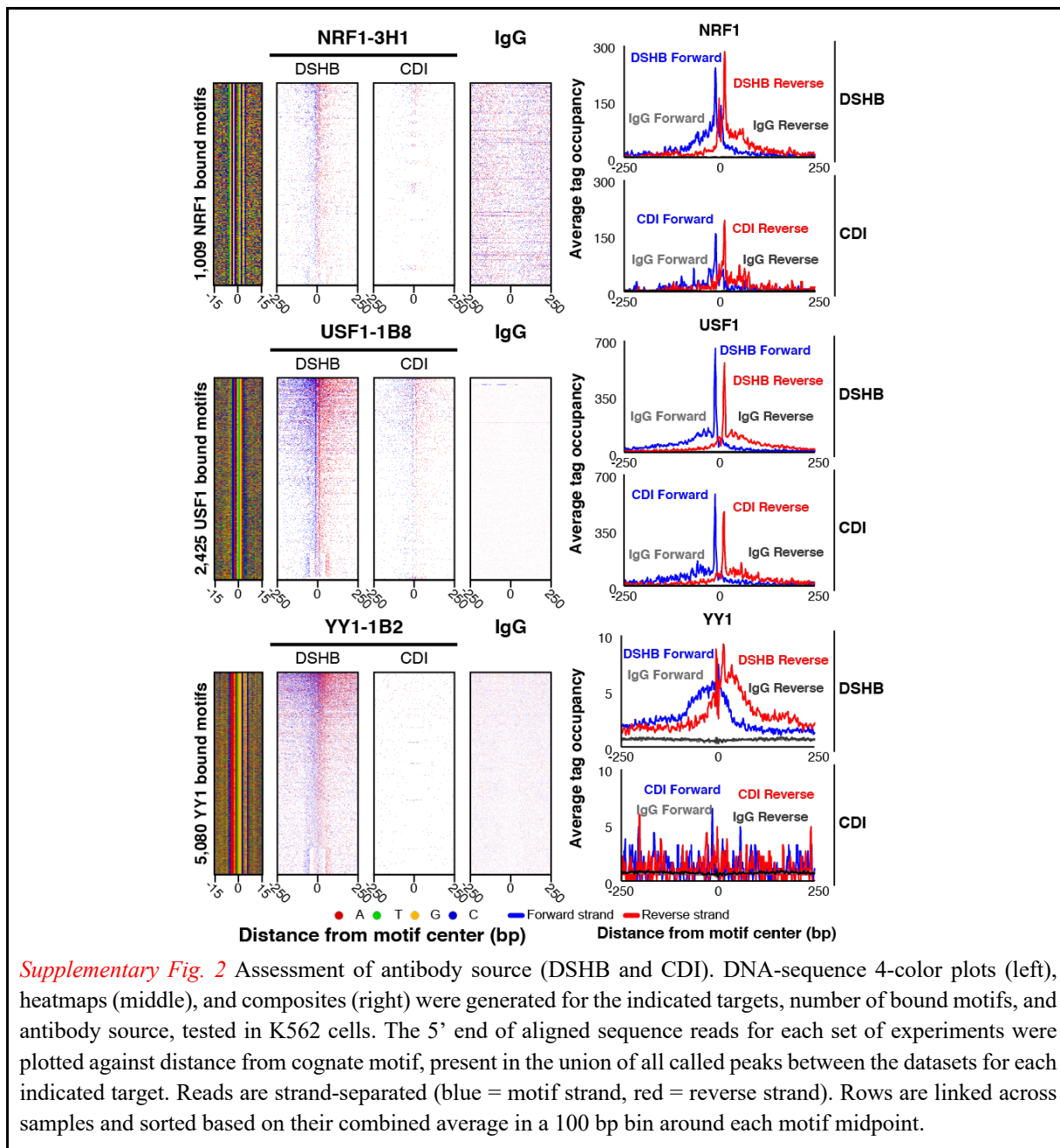
196



197
198
199
200
201
202
203

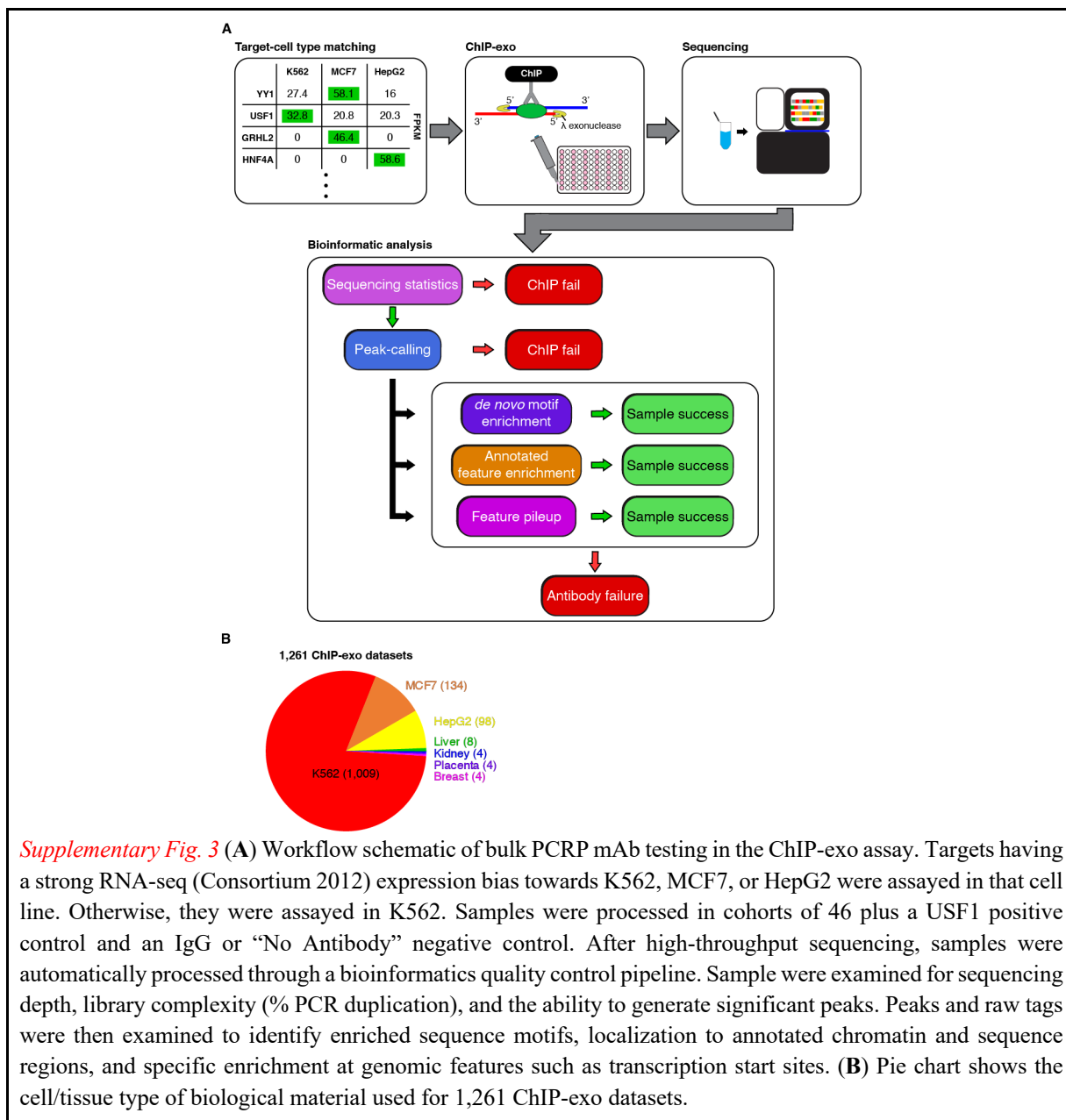
We first examined vendor source. We tested NRF1, USF1, and YY1 PCRp mAb from DSHB and CDI. The former was supplied as hybridoma culture supernatants (10-80 ug/ml antibody), and the latter as concentrates (*Supplementary Fig. 2*). Each preparation (as supplied) was pre-loaded onto protein A/G magnetic beads. In general, we found that while mAbs from both sources (assayed at the same reported mAb amounts; 3 ug) specifically detect NRF1 and USF1, DSHB-derived hybridoma culture supernatants detected more binding events at cognate

204 motifs compared to CDI concentrates. We therefore sourced from DSHB for the remainder of
205 this study. Nevertheless, mAbs from CDI may be improved through further optimizations.
206



207
208 We assayed all 887 available hybridoma supernatants containing mAbs to 681 non-
209 redundant targets. Testing was initially performed in K562 (1,009 datasets), although a subset of
210 hybridoma supernatants were tested in MCF7 (134 datasets) and HepG2 (96 datasets) cells,
211 based on reported target mRNA expression levels. If there was no substantial difference in ssTF
212 expression level, or the ssTF was not measurably expressed in any of these three lines, testing
213 defaulted to K562 due to practical considerations including the ability to grow this line at scale
214 (liquid culture) (*Supplementary Fig. 3A*). 245 unique hybridoma clones were assayed in replicate

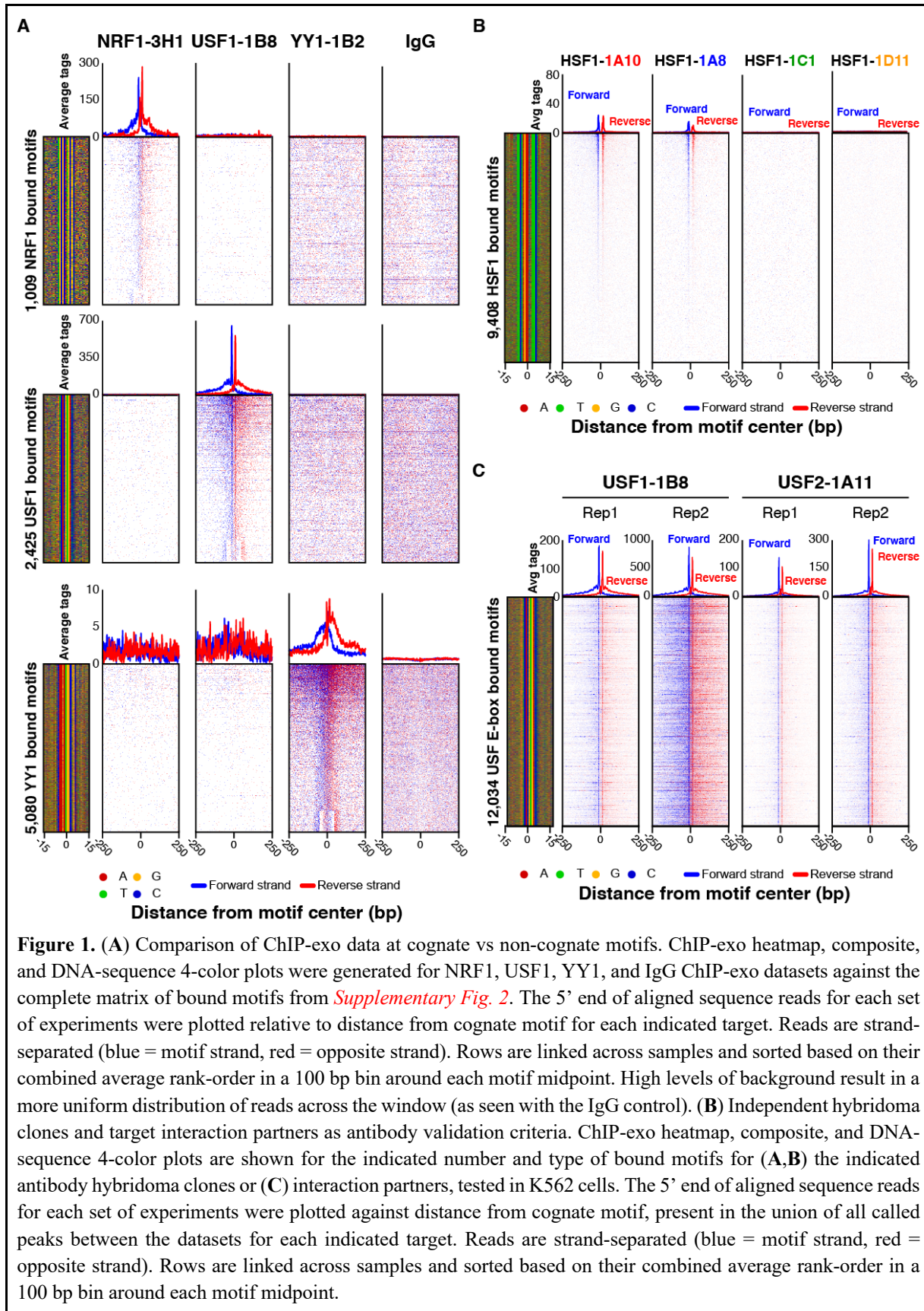
215 at least twice in the same or different cell types, resulting in 1,261 datasets (*Supplementary Fig.*
 216 *3B*). Of these 245 hybridoma clones, 36 (14.7%) showed enrichment of the same class of
 217 genomic features. 102 (41.6%) of the mAb clones produced no enrichment of genomic features
 218 in both replicates, and 107 (43.7%) produced enrichment in one sample but not in the other
 219 (*Supplementary Table 1*). The latter may be due to being at the limits of detection. We next set
 220 out to characterize certain mAb in more depth.
 221

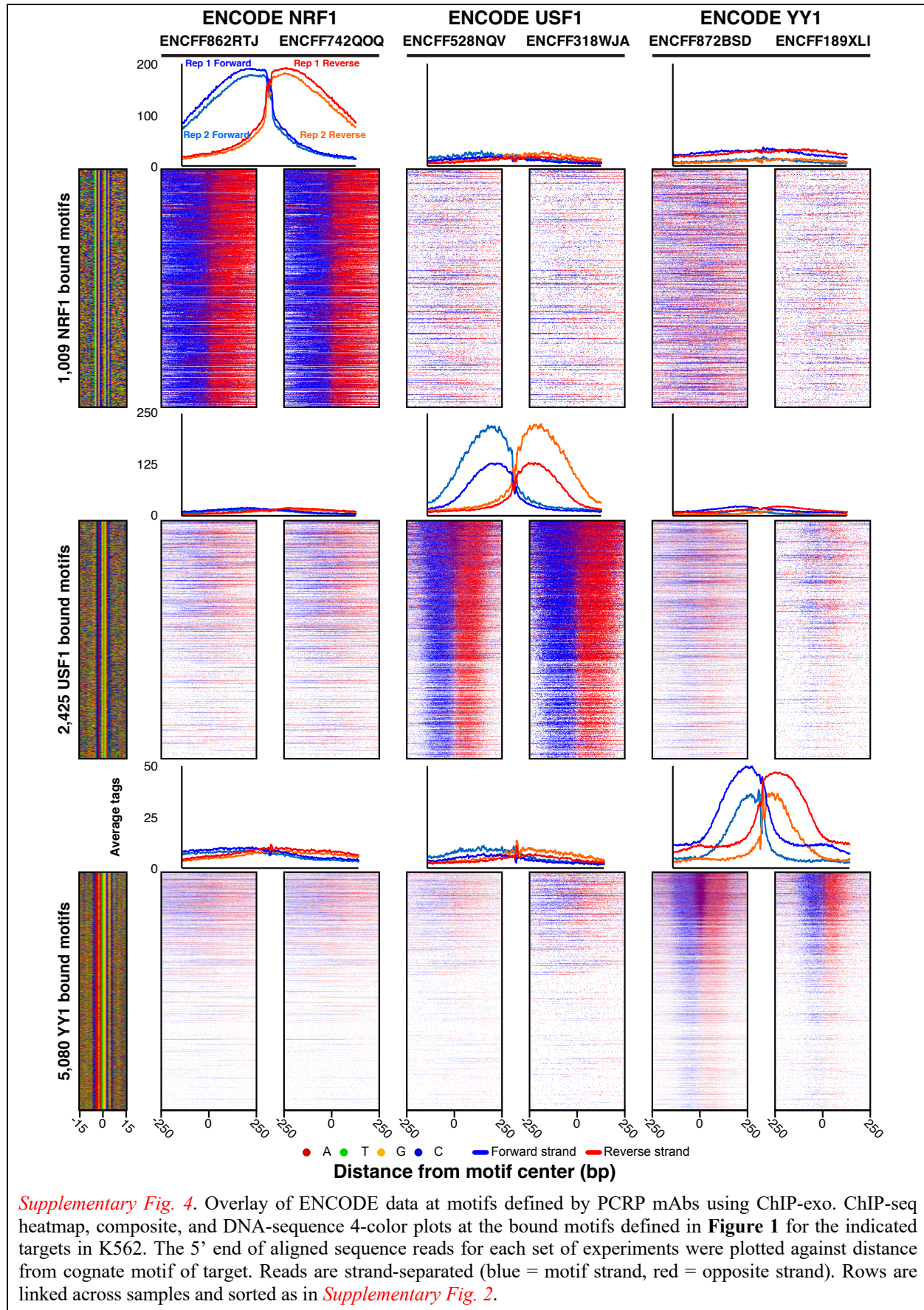


222
 223 As exemplified by NRF1, USF1, YY1, and an IgG negative control (**Figure 1A**), the
 224 finding that ChIP-exo peaks were enriched at a very precise distance from cognate motifs
 225 provided strong support for specificity in target detection. We also compared different
 226 hybridoma clones against the same target, as exemplified by heat shock factor 1 (HSF1).

227 Hybridoma clones potentially target different epitopes, although immunodominance may yield
228 independent clones to the same epitope. Both HSF1 mAbs gave nearly identical ChIP-exo read
229 patterns around the same set of features (heat shock elements, **Figure 1B**, clones 1A10 and 1A8),
230 thereby demonstrating reproducibility of ChIP-exo profiles across independent PCRPs mAbs.
231 This is particularly important where validation criteria by motif enrichment are not applicable.
232 However, two other HSF1 mAb clones failed (**Figure 1B**, clones 1C1 and 1D11), indicating that
233 independent PCRPs clones can have different capabilities in ChIP. Therefore, if one mAb clone
234 fails, it may be productive to check others.

235 Targets that interact with each other or with the same sites may also provide a useful
236 validation criterion for determining enrichment specificity. For example, in the case of USF1 and
237 USF2 interaction partners and homologs (Rada-Iglesias et al. 2008), the USF1-1B8 and USF2-
238 1A11 mAbs detected binding at the same sites (**Figure 1C**). However, in this particular case we
239 cannot exclude cross-reactivity of the mAb with the two homologous USF1/2 proteins (always a
240 potential concern with target-specific antibodies). Additional validation criteria may include
241 comparisons to public-domain ChIP-seq datasets that use different antibodies (*e.g.*, ENCODE, as
242 in *Supplementary Fig. 4*).

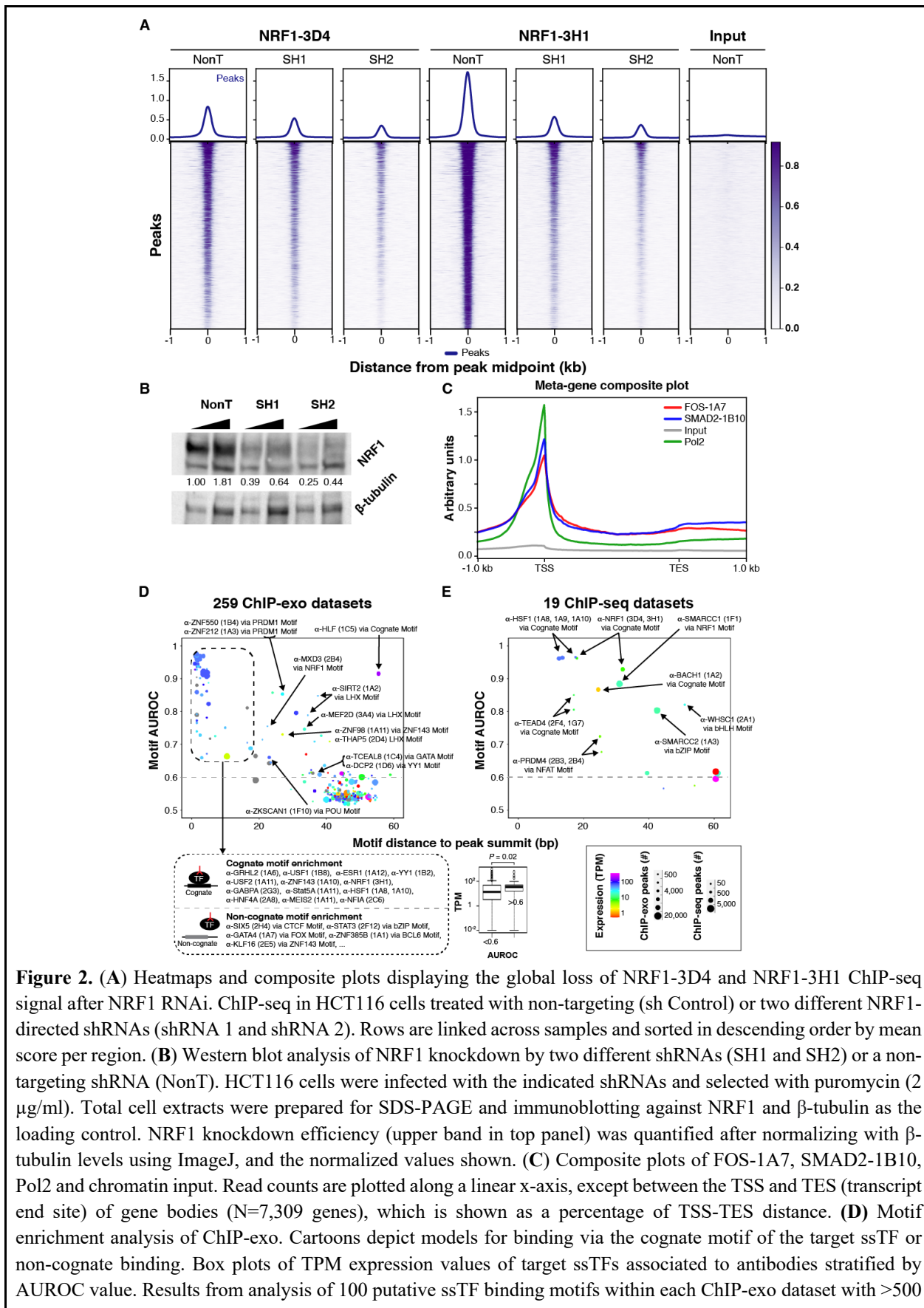




244 **Assessment by ChIP-seq**

245 Since ChIP-seq is a widely used assay (and related to ChIP-exo), we performed ChIP-seq
246 (in HCT116 cells) with 137 PCRPs hybridomas corresponding to 70 targets associated with
247 chromatin binding, modification, enhancer function, and/or transcriptional elongation. We found
248 19 (14%) produced significantly enriched peaks (see Methods) (*Supplementary Table 2*).
249 However, these single-replicate datasets were not checked for enrichment of specific classes of
250 genomic features. Stringent validation for antibody-specificity involves knocking down a target,
251 then observing a reduction of assayed signal relative to a mock knockdown (Wardle and Tan
252 2015; Uhlen et al. 2016; Edfors et al. 2018). We examined the feasibility of this starting with one
253 target, NRF1. NRF1 expression was knocked down in HCT116 cells by RNAi. NRF1 peaks
254 were concomitantly diminished with two different specific oligos, but not by an untargeted oligo
255 (**Figure 2A**), thereby demonstrating specificity of the PCRPs mAbs 3D4 and 3H1 for this target.
256 We further confirmed specific knockdown of NRF1 by immunoblot (**Figure 2B**). Due to the
257 relatively high cost and current limitations in knock-down technologies, we found it was not
258 practical within the scope of this project to conduct systematic knockdowns across the PCRPs
259 mAb collection. Furthermore, knockdown validation may not provide the level of validation
260 stringency in ChIP that it does for immunoblots. Knockdown of proteins can cause widespread
261 indirect effects on the binding of other protein-complexes which could in turn skew the ChIP-
262 signal in aberrant ways (Trescher and Leser 2019).

263 Two mAbs (FOS-1A7 and SMAD2-1B10) gave unexpected ChIP-seq patterns for their
264 intended targets; namely enrichment at transcription start sites (TSS in **Figure 2C**). Previous
265 studies have shown SMAD2 and FOS binding predominately occurs within active enhancers and
266 not at TSS (Aragon et al. 2019; Su et al. 2020). However, both ChIP-seq and ChIP-exo showed
267 enrichment at TSSs and not at predicted (chromHMM) enhancers (see also online data). Deeper
268 biochemical validation will be needed to verify the specificity of these mAbs.



peaks (259 datasets in total). We assigned to each ChIP-exo dataset the PWM with the highest AUROC (“Top Motif”) and quantified its centering as the mean distance of the PWM match from the peak’s summit. In the scatter plot, each point represents the enrichment/centering of the top motif in one of the 259 putative TF ChIP-exo datasets. Colors indicate the expression level (RNA-seq TPM value (Consortium 2012); unavailable values are shown in gray) of the gene specific for the antibody used in the ChIP assay. Point sizes indicate the number of ChIP-exo peaks in the dataset. Top motifs with AUROC >0.6 (dashed line) and TPM values from duplicate RNA-seq experiments are indicated. (E) Results from enrichment analysis of 100 TF binding motifs within each of 19 ChIP-seq datasets. Points are formatted as in (D).

269

270 **Assessment through feature enrichment**

271 Thus far we have established the utility of three independent validation criteria inherent
272 to ChIP-exo analysis: 1) enrichment and patterning at a cognate motif (**Figure 1A**); 2)
273 correlation with an independent mAb clone (**Figure 1B**); and 3) co-localization with an
274 interacting partner (**Figure 1C**). In our large-scale evaluation of mAbs, these validation criteria
275 often were either not applicable or not attainable. We therefore looked for additional criteria that
276 might be useful where the preferred validation criteria were inconclusive. We used the ChExMix
277 algorithm to identify significant modes of protein binding and *de novo* motif detection through a
278 combination of DNA sequence enrichment and variation in ChIP-exo patterning (Yamada et al.
279 2019). Discovered motifs were identified using TOMTOM and the JASPAR database (Gupta et
280 al. 2007; Fornes et al. 2020). Next, their relative enrichment in annotated genomic regions (e.g.,
281 promoters, enhancers, and insulators) was quantified. Enrichment may be suggestive of function.
282 These included chromHMM and Segway genome segmentations (*Supplementary Fig. 3A*)
283 (Hoffman et al. 2013).

284 We also considered a low stringency test that did not require statistical enrichment of
285 peaks (useful for low coverage). Composite plots were generated around well-defined general
286 features like transcription start sites and CTCF binding sites and the average tag enrichment was
287 examined relative to a negative control (IgG) background. We caution that any enrichments for
288 particular targets relative to these features should be followed up with additional replicates. Test
289 results for all validation criteria and other analyses for each tested antibody can be found at
290 www.PCRPvalidation.org and *Supplementary Table 1*. The website provides a deep and rich
291 resource for preliminary discovery for each target, particularly since the vast majority of targets
292 remain uncharacterized (at all, or in the manner(s) we have performed). We caution that the
293 website provides automated analysis for all datasets, including those that did not pass our
294 significance thresholds and/or were not replicated independently. Some of these may simply
295 reflect non-optimized ChIP conditions (e.g., antibody amounts and/or cell type). These additional
296 analyses generally offered less confidence compared to *a priori* cognate motif validation because
297 many of the defined chromatin states are relatively abundant in the genome. The analyses should
298 serve only as a reference point for additional characterization and optimization, and not used to
299 draw biological conclusions.

300

301 **Evaluation through motif analysis**

302 To further evaluate the ChIP-exo and ChIP-seq data for evidence of ssTF genomic
303 occupancy (direct or indirect), we analyzed 259 ChIP-exo and 19 ChIP-seq peak files for ssTF
304 motif enrichment by using an Area Under the Receiving Operator Characteristics curve
305 (AUROC) metric in which ChIP ‘bound’ regions are compared to a background set of unbound
306 sequences. Briefly, the AUROC assesses the enrichment of matches to a given TF motif among
307 the ChIP ‘bound’ regions as compared to a background set of unbound regions; the resulting
308 AUROC value ranges from 0 to 1, with 0.5 corresponding to that expected at random. In addition
309 to AUROC motif enrichment, we also quantified the distance of the motif to the peak summit,
310 which is expected to be shorter for motifs recruiting the profiled ssTF to the DNA (either directly
311 or through a tethering ssTF partner) (Gordan et al. 2009; Bailey and Machanick 2012; Wang et
312 al. 2012; Mariani et al. 2017) (**Figure 2C,D**). We used a collection of 100 non-redundant
313 position weight matrices (PWMs) representative of the known repertoire of human ssTF binding
314 specificity (Bailey and Machanick 2012). These approaches identified 20 PCRPs antibodies,
315 corresponding to 16 putative ssTFs, for which their cognate DNA motif was both enriched and
316 centered within the ChIP peaks (“Direct Binding” in *Supplementary Table 3*). Possible reasons
317 for the remaining datasets not showing significant motif enrichment include (but are not limited
318 to): (i) the target TF was not expressed at sufficiently high levels or at sufficiently high nuclear
319 concentrations in the assayed cells, (ii) the epitope recognized by the antibody was not accessible
320 in the chromatin context in the assayed cells, (iii) the target TF was not occupying specific
321 genomic target sites (either directly or indirectly) in the assayed cells, or (iv) off-target
322 recognition by the antibody of other proteins in the assayed cells, resulting in lack of sufficient
323 enrichment of the intended target TF.

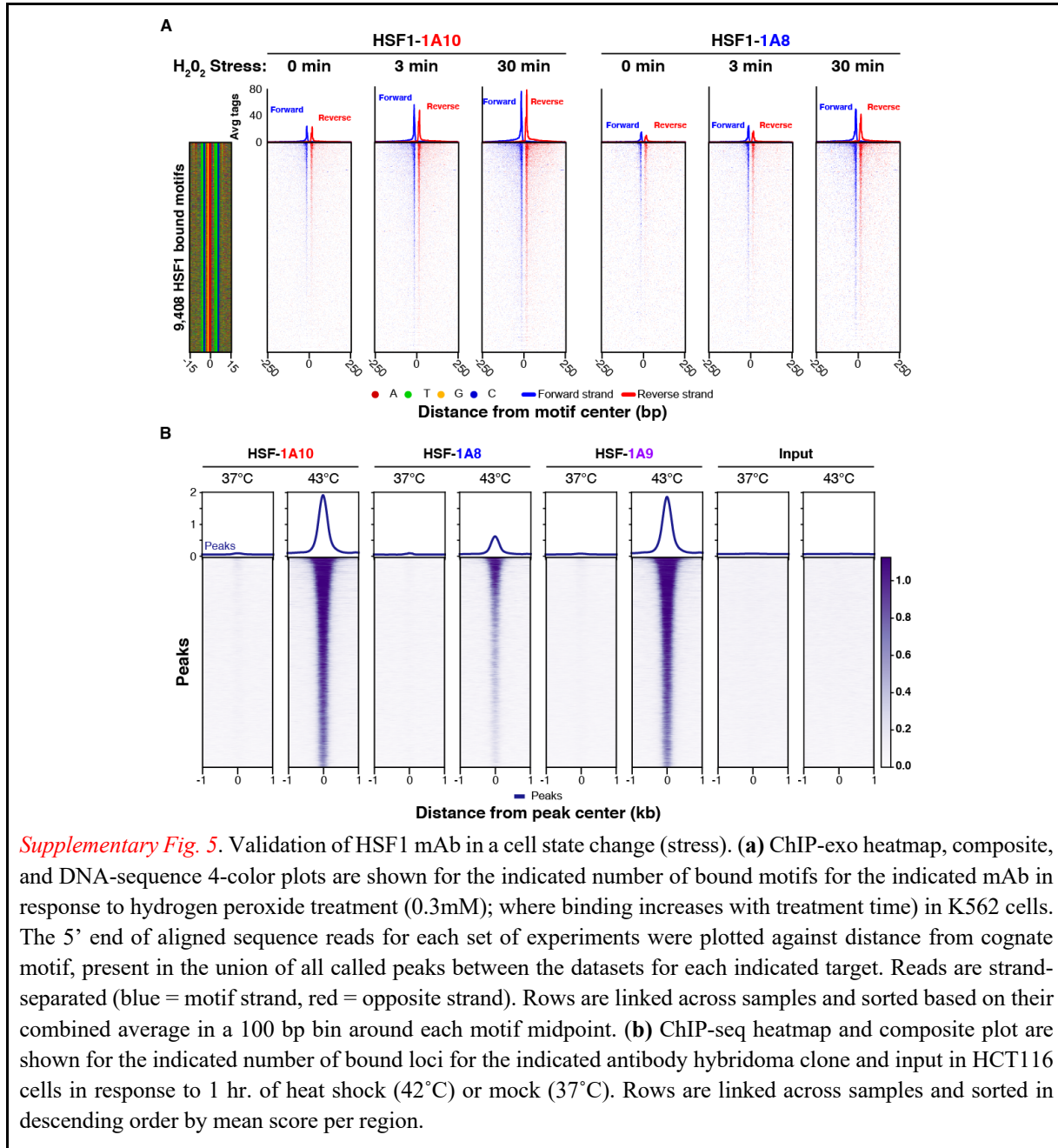
324 Of the analyzed datasets, an additional 30 PCRPs mAbs showed enrichment for a binding
325 motif other than the cognate motif of the ChIP-profiled ssTF (**Figure 2C,D**). The enrichment of
326 a non-cognate motif suggests that the genomic occupancy of the ChIP-profiled ssTF might be
327 mediated through indirect binding by a different ssTF (Wang et al. 2012; Mariani et al. 2017),
328 which is bound directly to those ChIP ‘bound’ genomic sites through the enriched motif
329 (“Indirect Binding” in *Supplementary Table 3*). In this way, we have previously identified
330 indirect binding modes from ChIP-chip or ChIP-seq experiments that used traditionally prepared
331 antibodies against either an epitope tag on yeast ssTFs or human ssTFs (Gordan et al. 2009;
332 Mariani et al. 2017). Here, for example, the NFAT motifs was enriched and centered among
333 ChIP-seq peaks resulting from ChIP-seq experiments using two different anti-PRDM4 PCRPs
334 antibody clones (2B3 and 2B4), suggesting that in HCT116 cells PRDM4 binds DNA indirectly
335 via an NFAT factor. As none of the indirect binding modes that we inferred in this study have
336 been described previously to our knowledge, future experiments are needed to verify them and to
337 rule out the alternative possibility that the antibody may preferentially cross-react with a TF
338 whose motif was found enriched.

339

340 **ChIP assessment in multiple cell states and types**

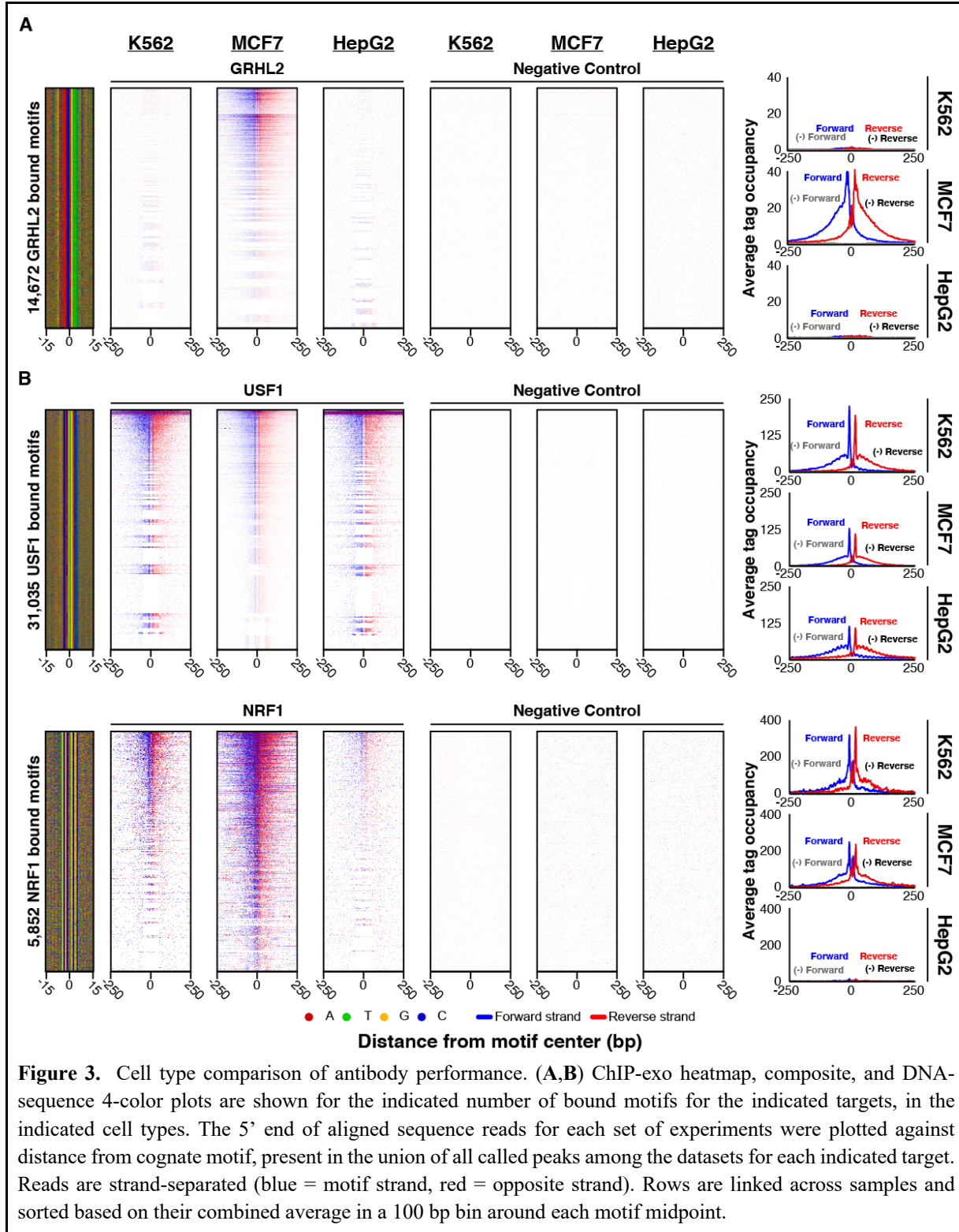
341 Any number of targets may be sequestered in a state that prevents their interaction with
342 chromatin (and thus detection by ChIP) unless activated to do so through a change in cell state.
343 We examined this with HSF1, which is rapidly induced to bind in the nucleus upon heat shock to

344 activate heat shock response genes (Baler et al. 1993). HSF1 was bound to cognate motifs at
 345 relatively low levels under non-stressed conditions but increased in binding upon treatment of
 346 cells with hydrogen peroxide (0.3 mM) for 3 min and 30 min. (*Supplementary Fig. 5A*, assayed
 347 by ChIP-exo), or upon heat shock (shift from 37°C to 42°C for 1 hr) (*Supplementary Fig. 5B*,
 348 assayed by ChIP-seq). This illustrates a potential problem with using mRNA expression levels as
 349 a basis for expecting a factor to be actively bound to chromatin. Many TFs are sequestered and
 350 only bind chromatin when released by signaling events.
 351



352 While ChIP-exo antibody assessments were primarily performed in K562 cells (see
 353 above), many targets may have chromatin interactions that are cell-type specific. An example of
 354 cell-type specific expression was observed with the breast cancer factor GRHL2, where binding

355 was detected in MCF7 cells but not in other cell types (**Figure 3A**). Other targets like USF1 and
 356 NRF1 were less cell type-specific, although we do not exclude selectivity at subsets of sites
 357 (**Figure 3B**). Therefore, testing antibodies in the appropriate cell type (with appropriate signaling
 358 events) may be critical for target detection.



360 We next tested a subset of PCRPs mAbs on donated de-identified human organs. ChIP-
361 exo was performed using mAbs against USF1, YY1, and GABPA in chromatin from human liver
362 (2 different specimens), kidney, placenta, and breast tissue (**Figure 4**). Largely consistent with
363 the cell line ChIP's, enrichment and aligned read patterning was observed with all three mAbs
364 for the liver and kidney, that was diminished in placenta and not detectable in breast. It remains
365 to be determined whether the lack of signal in breast is due to technical limitations in chromatin
366 yields versus tissue specificity of chromatin interactions. Nonetheless, these findings
367 demonstrate the utility of at least some PCRPs mAb in epigenomic profiling of human clinical
368 specimens.
369

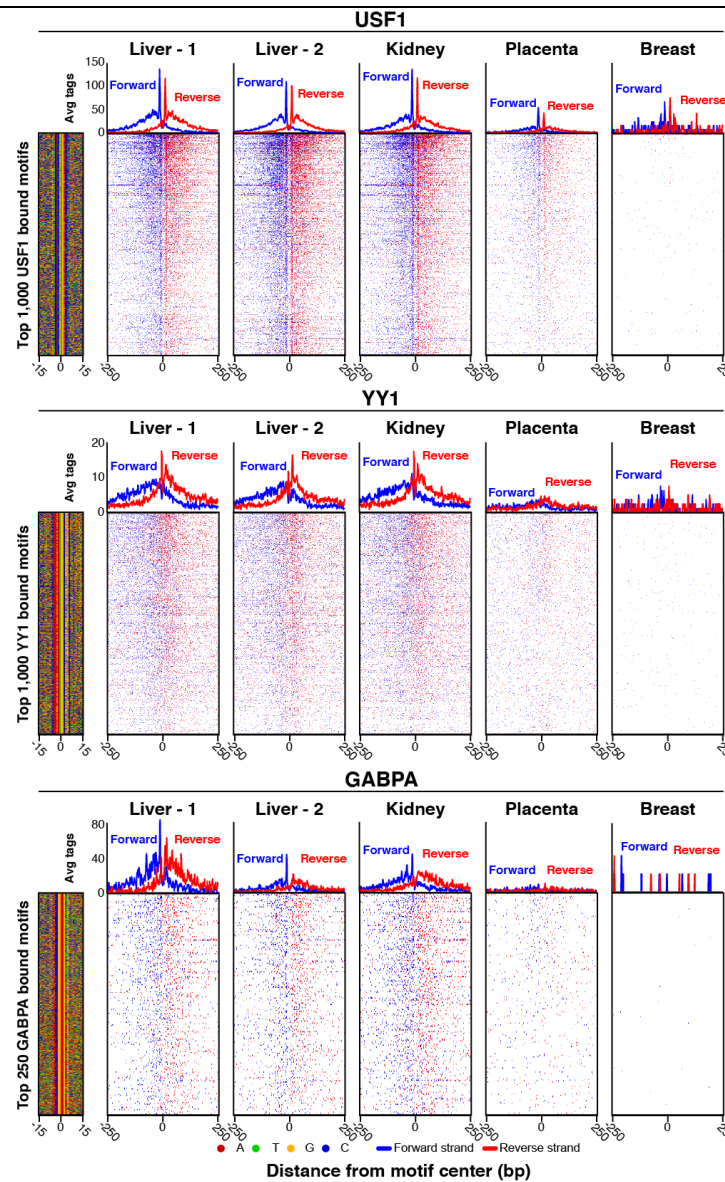
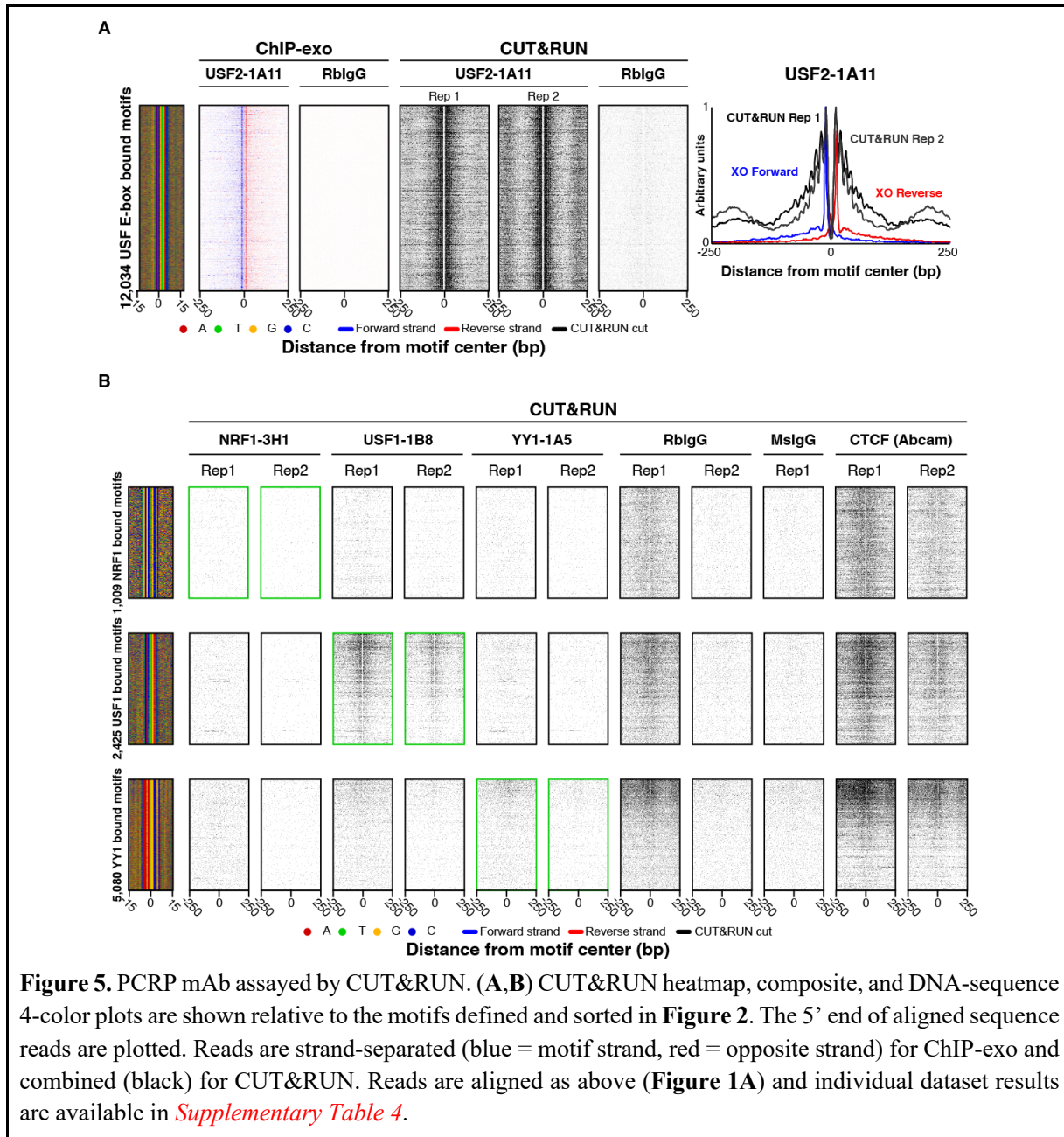


Figure 4. Application of ChIP-exo in human tissue using PCRPs mAbs. ChIP-exo heatmap, composite, and DNA-sequence 4-color plots are shown for the indicated number and type of bound motifs for the indicated targets, in the indicated organ types (liver includes two donors). The 5' end of aligned sequence reads for each set of experiments were plotted against distance from cognate motif, present in the union of all called peaks between the datasets for each indicated target. Reads are strand-separated (blue = motif strand, red = opposite strand). Rows are linked across samples and sorted based on their combined average in a 100 bp bin around each motif midpoint.

370

371 **Evaluation using CUT&RUN.**

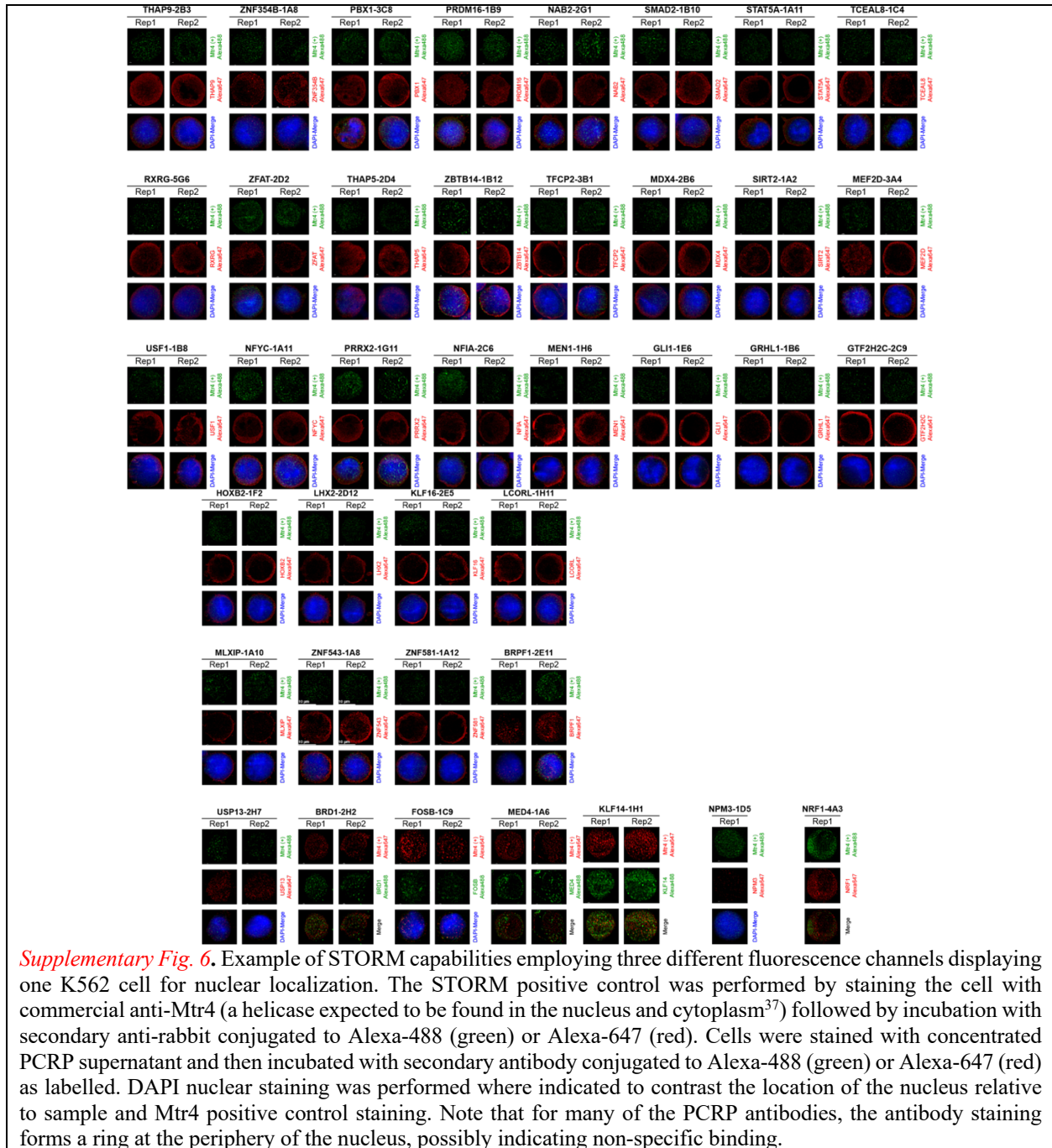
372 CUT&RUN has been used to measure genome-wide protein-DNA interactions (Skene et
373 al. 2018). It uses a fusion of protein A/G (pAG; which binds most antibody isotypes in common
374 use) and micrococcal nuclease (MNase). A ssTF-specific antibody is added to immobilized
375 permeabilized cells or nuclei (under native or crosslinked conditions), where it binds to its
376 chromatin target. pAG-MNase is next added, recruited via pAG to the target-specific antibody,
377 and the MNase portion cleaves local DNA. The result is a selective release of chromatin from the
378 otherwise insoluble nucleus, where genomic enrichment can be identified by sequencing. We
379 tested 40 PCRPs antibodies in K562 by native CUT&RUN in replicate (see Methods), of which
380 25 had been selected based on ChIP-exo enrichment. For USF2, NRF1, USF1, and YY1, we
381 mapped CUT&RUN cleavage sites around their ChIP-exo detected cognate motifs. Multiple
382 nonspecific IgGs served as the negative controls. As additional negative controls, we mapped
383 DNA cleavages around this same set of motifs using the other noncognate ssTF datasets, where
384 only background cleavage is expected (as we did for ChIP-exo in **Figure 1** and ChIP-seq in
385 *Supplementary Fig. 4*). Of all 40 PCRPs antibodies tested, USF2-1A11 produced the most
386 robust CUT&RUN signal (**Figure 5A**), with a detection level matching ChIP-exo, and low IgG-
387 only background. Thus, the native CUT&RUN assay as implemented here has the ability to
388 detect site-specific protein-DNA interactions through at least one PCRPs mAb. However, for the
389 NRF1, USF1, and YY1 mAbs, which had worked well in ChIP-exo, we observed little or no
390 enrichment above background in native CUT&RUN (**Figure 5B**). This may reflect intrinsic
391 target incompatibility with the native approach, or that antibody-specific optimization is
392 warranted. Analysis results for the remaining CUT&RUN datasets and controls are in
393 *Supplementary Table 4*. Of note, a DNA-accessibility footprint was observed in some negative
394 control experiments, including a CTCF dataset at noncognate CTCF locations (e.g., at NRF1 and
395 USF1 motifs in **Figure 5B**). This may indicate background cleavage by untargeted pAG-MNase
396 at TF binding sites, perhaps due to the open chromatin at these locations or an intrinsic MNase
397 sequence bias and demonstrates the importance of controls with the CUT&RUN approach.
398 Background cleavage intensity may also vary based on the amount and type of IgG used in the
399 negative control, making peak-calling less reliable. Thus, cognate target specificity in most of
400 these CUT&RUN experiments was not established.



401

402 Evaluation by STORM

403 As part of our PCRp mAb evaluation, we performed Stochastic Optical Reconstruction
 404 Microscopy (STORM), which can visualize cellular structures / processes at nanometer
 405 resolution (Betzig et al. 2006). The approach involves the use of fluorescently conjugated
 406 antibodies that might be expected to bind identifiable structures in specific subcellular
 407 compartments. Of the 39 PCRp mAbs surveyed (*Supplementary Table 5*), most displayed peri-
 408 cytoplasmic staining, rather than expected punctate nuclear staining (*Supplementary Fig. 6*).
 409 Thus, without further supporting evidence, these results were inconclusive. However, we provide
 410 these images as comparison datasets for future studies.

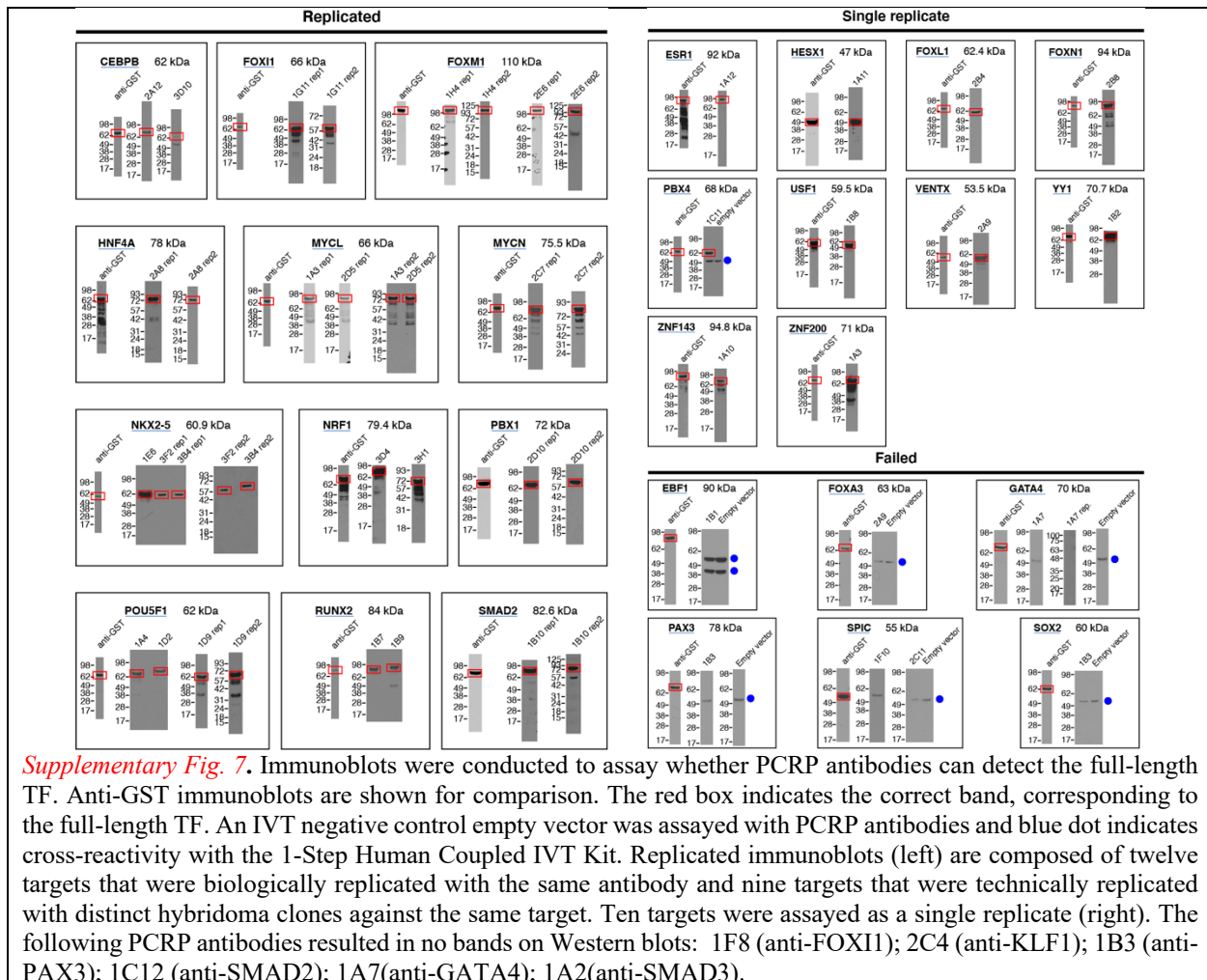


411

412 Evaluation using *in vitro* binding assays

413 We next tested 44 PCR mAbs by *in vitro* protein binding assays. A classic method to
 414 evaluate antibody specificity is western blotting: size separation of complex protein mixtures
 415 using denaturing gel electrophoresis (SDS-PAGE), followed by membrane transfer, and
 416 immunoprobing with an antibody of interest to determine the protein species it detects. Since
 417 endogenous targets can exist at a level below the sensitivity of detection, we used coupled-*in*
 418 vitro transcription/translation (IVT) in crude HeLa cell extracts to produce 32 TFs as unpurified
 419 amino-terminal GST-fusion proteins (*Supplementary Table 6*). This allowed for production of
 420 higher levels of target proteins, but within a complex *milieu* of other proteins to allow specificity

421 to be addressed. Of the 44 PCRPs mAbs assayed by immunoblotting, 31 (70%) mAbs detected a
 422 single predominant band of the expected molecular weight (twelve as biologically independent
 423 replicates of the same antibody, plus nine replicated with a different mAb, plus ten performed as
 424 a single replicate, *Supplementary Fig. 7*). As a positive control, anti-GST antibody detected 32 of
 425 the 33 GST-fusion TFs. Thus, about two-thirds of the assayed PCRPs mAbs were specific in
 426 recognizing their target proteins. This success rate (70%) may represent the upper limit of
 427 success for these reagents.
 428



429
 430 Protein binding microarrays (PBMs) is a technique to assay protein-DNA binding
 431 specificity *in vitro* (Mukherjee et al. 2004; Berger et al. 2006; Siggers et al. 2011b). Proteins
 432 used in PBMs are typically expressed as epitope tag-fusions, supporting detection on the DNA
 433 array by fluorescent anti-tag antibody. A possible explanation for why some antibodies may fail
 434 to work in ChIP experiments is that their target epitope may become inaccessible when the ssTF
 435 is bound to a protein partner, DNA ligand, and/or subjected to modification by formaldehyde.
 436 Therefore, for a set of 31 ssTFs that were of interest or performed well in ChIP, we used PBMs
 437 to test 44 PCRPs mAb for their ability to recognize their DNA-bound target TF.

438 Briefly, the relevant IVT-generated TFs were incubated with DNA microarrays where all
 439 possible 10-bp sequences were represented within ~44,000 60-bp probes on double-stranded
 440 oligonucleotide arrays (Agilent) (Berger et al. 2006). For 20 of these 44 PCRPs mAbs (45%)
 441 assayed against 16 of 22 tested targets, the PBM experiments successfully identified a DNA
 442 binding motif consistent with the known or anticipated element (**Figure 6**). All mAb PBM
 443 experiments were run with a parallel anti-GST antibody (positive control) to validate the
 444 viability of the IVT-expressed target in PBM resulting in a 21/22 (95%) validation rate. Of the
 445 20 PCRPs antibodies that successfully yielded the expected motif in PBMs, 11 (55%) had at least
 446 some validation support by ChIP.
 447

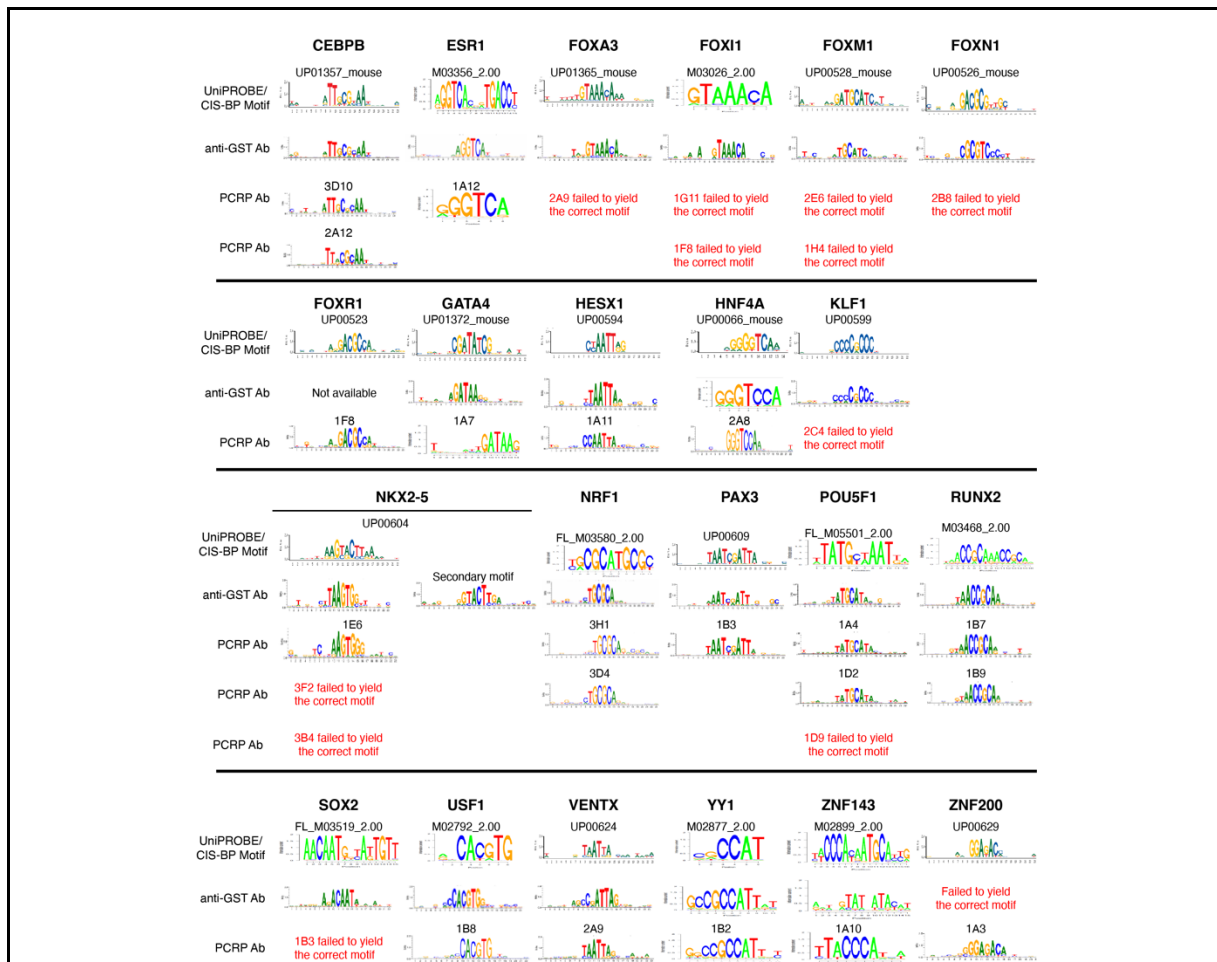


Figure 6. TF binding motifs derived from PBM experiments performed using anti-GST or PCRPs antibodies. Each full-length TF was assayed with its PCRPs mAb(s) and compared against its corresponding motif derived from an anti-GST PBM experiment and anticipated motif from the UniPROBE or CIS-BP databases (Weirauch et al. 2014; Hume et al. 2015). The TFs from UniPROBE or CIS-BP were assayed as extended DNA binding domains. For display of sequence motifs, probability matrices were trimmed from left and right until 2 consecutive positions with information content of 0.3 or greater were encountered, and logos were generated from the resulting trimmed matrices using enoLOGOS (Workman et al. 2005).

449 **Discussion**

450 The ability to interrogate the diverse human proteome is heavily reliant on specific
451 affinity capture reagents, of which antibodies are the most widely used. PCR²P represented a pilot
452 project for the entire human proteome, with initial focus on nuclear proteins. To this end, this
453 study assayed nearly all PCR²P mAb against ~700 putative chromatin targets or TF using the
454 genome-wide high resolution ChIP-exo assay. A smaller subset was analyzed by other genome-
455 wide assays (ChIP-seq, CUT&RUN); super-resolution microscopy (STORM); to directly detect
456 recombinant target proteins by immunoblotting; or their DNA-binding by PBMs. Our purpose is
457 to present a technical “field” assessment of PCR²P mAb utility in biochemical and cellular assays.
458 Given the published rigorous criteria for antibody validation (Landt et al. 2012; Wardle and Tan
459 2015; Uhlen et al. 2016; Edfors et al. 2018; Sikorski et al. 2018), which may be assay specific,
460 this work is not intended to provide a comprehensive resource of validated antibodies. Instead, it
461 is a starting point for considering validation criteria and any limits that may be applicable to
462 particular assays, especially when taking a systematic high-throughput approach. ChIP-exo
463 identified up to 5% of the ~1,000 tested PCR²P antibodies as having high specificity for their
464 targets, based on orthogonal evidence of motif enrichment and other criteria. These reagents
465 would be the strongest candidates for more rigorous validation testing.

466 In contrast, a large number of PCR²P mAbs did not meet the defined validation criteria we
467 employed. We suggest that some producing ambiguous outcomes might benefit from assay
468 optimization: e.g., a different cell type or growth condition in which the target is expressed
469 and/or activated for chromatin binding. Additionally, different metrics or validity thresholds may
470 be needed. Notably, many of the PCR²P mAbs were evaluated by ChIP-exo in K562, while their
471 target TFs may not be appreciably expressed in these cells. However, as shown for HSF1, even
472 where a target is expressed, it may not substantially interact with chromatin (and thus escape
473 detection) unless activated to do so. Therefore, knowledge of the underlying biology of the target
474 may be critical in how ChIP specificity is assessed.

475 Several algorithmic explanations can be considered for lack of target detection. Some
476 sequence-specific DNA binding proteins may not have been accommodated within our discovery
477 framework. For example, a target protein may bind a nonstandard distribution DNA sequences
478 that was not captured by current motif discovery algorithms. Alternatively, the target may
479 interact with a wide range of genomic sites having different or degenerate DNA sequence motifs
480 (including indirect sequence readout based on DNA shape (Rohs et al. 2009)) that are not
481 accommodated by the discovery algorithms used in this study. Another possible scenario is that a
482 target protein might not bind DNA directly, but only indirectly through other proteins, including
483 those that potentially form an undiscovered chromatin class (which would not be in our
484 discovery pipeline). We often found motifs that were long, simple, semi-repetitive, and highly
485 degenerate (see online). These are not typical properties of sequence-specific DNA binding
486 proteins and the ChIP-exo patterns at these motifs were often quite distinct from well-validated
487 targets. Historically, some of these locations may have been set aside as problematic, and thus
488 excluded from analysis (Consortium 2012). Whether these regions are artifactual or have some
489 unknown biology remains to be determined. While we accepted these motifs as evidence of
490 enrichment, we urge caution when interpreting such atypical binding events.

491 It was not practical in our high-throughput ChIP-exo screen to profile each PCRPs mAb in
492 a wide range of cell types. However, for ssTFs with at least 500 significant peaks, we noticed an
493 association between the expression of the target proteins and the detection of binding motif
494 specificity (box plot in **Figure 2D**), and so expression may be a useful preliminary guide for cell-
495 type selection. Furthermore, some targets may simply not be cross-linkable to chromatin in the
496 assayed cell type (or any cell type), making ChIP an inappropriate assay. Unlike engineered
497 epitope tags, each target-specific antibody may have a substantially different affinity for its
498 cognate antigen. Therefore, we cannot rule out that at least some low- or non-performing
499 antibodies could perform better under different immunoprecipitation conditions. Still other
500 potential reasons for antibody non-performance may be due to trivial explanations like lot
501 expiration or mis-labeling along the supply chain.

502 In total, 946 unique hybridoma clones were tested in at least one of the assays. We
503 identified 50 clones (5%) that worked with high confidence in at least one assay. However, only
504 a very small portion of the validation spectrum has been explored. Using relaxed criteria, that
505 may reflect significant but off-target or unknown behavior, we find that 371 (39%) of the tested
506 PCRPs mAb had at least some evidence of being different from background, in at least one assay.
507 However, such marginal criteria require deeper characterization, such as target depletion/deletion
508 or negative control cell lines for a more robust validation. The remaining 61% also warrant more
509 testing in other cell types and conditions. Our analysis identifies an initial set of prioritized
510 candidates. A detailed summary of each assay's results along with all of the measured quality
511 control metrics is available in **Table 1**, along with an interactive searchable web-interface online
512 at www.PCRPvalidation.org.

513

514 **Methods**

515 **ChIP protocols**

516 *Antibodies.* 1,308 TF hybridomas were reported through the PCRPs portal at the start of
517 this study (September 2017). Hybridoma supernatants were purchased from Developmental
518 Studies Hybridoma Bank (DSHB, U. Iowa, IA) as 1 ml aliquots. Monoclonal antibody (mAb)
519 concentration averaged 36 ug/ml by ELISA quantification. Hybridoma supernatants contain
520 ADCF-mAb cell culture medium (<https://dshb.biology.uiowa.edu/tech-info>.) and residual (2%)
521 fetal bovine serum, which has a reported IgG concentration of 1-6 ug/ml (Son et al. 2001).
522 DSHB preparation dates were provided. Concentrated mAbs and their concentration were
523 generously provided by CDI laboratories (Mayaguez, PR).

524 *Cell material.* Cell stocks were obtained by the Pugh laboratory from ATCC. K562 were
525 grown in suspension using IMDM media and periodically checked for mycoplasma
526 contamination. HepG2 and MCF7 were grown as adherent cells in DMEM media. MCF7 cells
527 were additionally grown in phenol red-free DMEM and treated with Beta-estradiol 30 min prior
528 to cell harvest. Cells were pelleted, re-suspended in PBS, crosslinked with 1% formaldehyde for
529 10 min, and then quenched with a molar excess of glycine. Donated human organs were obtained
530 from NDRI (Philadelphia, PA) and then cryoground to fine powder using the SPEX cryomill
531 cryogrinder. Frozen tissue powder was re-suspended in room-temperature PBS containing
532 formaldehyde to a final concentration of 1% and quenched with a molar excess of glycine. All

533 cells and tissue for ChIP-exo then proceeded through standard lysis and sonication protocol
534 described below after crosslink quenching. HCT116 cells (ATCC CCL-247) were grown in the
535 Shilatifard laboratory in DMEM supplemented with 10% FBS (Fisher Scientific, 35-015-CV).
536 70%–80% confluent HCT116 cells were heat shocked for 1 hr by adding pre-heated conditioned
537 media pre-heated to 42°C (Lim et al. 2017). Heat shock and non-heat shock HCT116 cells were
538 washed with PBS before fixing with 1% formaldehyde (Sigma, 252549) in PBS for 15 minutes
539 and processing for ChIP-seq.

540 ChIP-exo testing was initially prioritized in K562, MCF7, and HepG2, using gene
541 expression values (FPKM in RNA-seq) generated from the ENCODE project as the basis for the
542 cell type used (Uhlen et al. 2005; Consortium 2012). Targets were assigned to the cell type most
543 likely to express the protein of interest. If no cell line had a clear high expression for a specific
544 target (>25% FPKM relative to all other considered cell lines), testing defaulted to K562. K562
545 was selected as the default due to its status as a Tier 1 ENCODE cell line and the plethora of
546 existing genomic data that could orthogonally support any findings. Samples were processed in
547 batches of 48 in 96 well plate format. The PCR-derived USF1 or NRF1 antibody served as a
548 positive control for every processed cohort as well as an IgG or “No Antibody” mock ChIP
549 negative control. Crosslinked sonicated chromatin from ~7 million cells was incubated with
550 antibody-bound beads, then subjected to the ChIP-exo 5.0 assay (Rossi et al. 2018).

551 *ChIP-exo 5.0 assay.* Chromatin for ChIP-exo was prepared by resuspending crosslinked
552 and quenched chromatin in Farnham cell lysis buffer at a ratio of 25 million cells to 1 mL of
553 buffer for 20 min at 4°C. At the 10 min mark, cells were pushed through a 25G needle 5 times to
554 enhance cellular lysis. Nuclei were then isolated by pelleting at 2,500g for 5min. Nuclei were
555 resuspended in RIPA buffer (25 million cells to 1 mL of buffer) for an additional 20 min at 4°C
556 and then pelleted again at 2,500g for 5 min. Disrupted nuclei were then finally resuspended in
557 1X PBS (25 million cells to 1 mL of buffer) and sonicated for 10 cycles (30on/30off) in a
558 Diagenode Pico. Solubilized chromatin was then processed through ChIP-exo. Production-scale
559 ChIP-exo 5.0 was generally performed in batches of 48 in a 96-well plate, alternating every
560 column to reduce risk of cross-contamination. Briefly, solubilized chromatin was incubated with
561 Protein A/G Dynabeads, preloaded with 3 ug of antibody, overnight then sequentially processed
562 through A-tailing, 1st adapter ligation, Phi29 Fill-in, Lambda exonuclease digestion, cross-link
563 reversal, 2nd adapter ligation, and PCR for final high-throughput sequencing. Equal proportions
564 of ChIP samples were barcoded, pooled, and sequenced. Illumina paired-end read (40 bp Read 1
565 and 36 bp Read 2) sequencing was performed on a NextSeq 500 and 550. While, on average, we
566 sought ~10 million total paired-end reads per ChIP, we accepted less if there was strong evidence
567 of target enrichment. Otherwise, we performed an additional round of sequencing. The 5' end of
568 Read_1 corresponded to the exonuclease stop site, located ~6 bp upstream of a protein-DNA
569 crosslink. Read_2 served two indirect functions: to provide added specificity to genome-wide
570 mapping, and to remove PCR duplicates.

571 *ChIP-seq.* 1×10^8 cells were fixed in 1% formaldehyde (Sigma, 252549) in PBS for 15-
572 20 min at room temperature and quenched with 1/10th volume of 1.25 M glycine for 5 minutes at
573 room temperature. Cells were collected at 1,000xg for 5 minutes, washed in PBS, pelleted at
574 1,000xg for 5 min and pellets were flash frozen in liquid nitrogen and stored at -80°C until use.

575 Pellets were thawed on ice and resuspended in 10 ml lysis buffer 1 (50 mM HEPES, pH 7.5, 140
576 mM NaCl, 1 mM EDTA, 10% glycerol, 0.5% IGEPAL CA-630, 0.25% Triton X-100 with
577 5µl/ml Sigma 8340 protease inhibitor cocktail incubated on ice 10 minutes, pelleted 1,500xg and
578 subsequently washed in lysis buffer 2 (10 mM Tris-HCl pH 8.0, 200 mM NaCl, 1 mM EDTA,
579 0.5 mM EGTA and 5ul /ml protease inhibitor) as with lysis buffer 1 before resuspending in 1 ml
580 lysis buffer 3 (10 mM tris-HCl pH 8.0, 1 mM EDTA, 0.1% SDS and 5 ul/ml protease inhibitors)
581 for sonication as previously described (Lee et al. 2006). Chromatin was sheared in a 1 ml
582 milliTUBE with AFA fiber on a Covaris E220 using 10% duty factor for 2 min. The
583 sheared chromatin concentration was estimated with Nanodrop at OD 260 and diluted to 1 mg/ml
584 in ChIP Dilution Buffer (10% Triton X-100, 1M NaCl and 1% Sodium deoxycholate). 1 mg
585 chromatin was combined with 4 µg hybridoma tissue culture supernatant and rotated overnight at
586 4°C. 40 µl of protein G Dynabeads was added and incubated for 2-4 hr rotating at 4°C. Samples
587 were washed 5 times with 1 ml RIPA buffer, 2 times with TE with 50 mM NaCl. Chromatin was
588 eluted with 800 µl elution buffer (50 mM Tris pH 8.0, 1 mM EDTA, 0.1% SDS) for 30 min at
589 65°C shaking at 1,500 rpm in a ThermoMixer (Eppendorf). Supernatants were collected,
590 digested with 20 µl of 20 mg/ml Proteinase K and incubated overnight at 65°C. DNA was
591 purified with phenol chloroform extraction. 500 µl of the aqueous phase was precipitated with 20
592 µl 5M NaCl, 1.5 µg glycogen and 1 ml EtOH on ice for 1 hr or at -20°C overnight.

593 Sequencing libraries were prepared with the KAPA HTP library prep kit (Roche) using 1-
594 10 ng DNA and libraries were size selected with AMPure XP beads (Beckman Coulter). Illumina
595 50 bp single-end read sequencing was performed on a NextSeq 500 or NovaSeq 6000. The
596 modular pipeline Ceto (<https://github.com/ebartom/NGSbartom>) was used to convert base calls
597 to fastq, align reads to bam files and make bigWig coverage tracks. Briefly, bcl2fastq with
598 parameters -r 10 -d 10 -p 10 -w 10 was used to generate fastq files. Trimmomatic version 0.33
599 with the options single end mode (SE) and -phred33 was used to remove low-quality reads.
600 Reads were then aligned to hg19 with Bowtie 1.1.2 (Langmead et al. 2009) with options -p 10 -m
601 1 -v 2 -S, thus keeping only uniquely mapped reads, and allowing up to two mismatches.
602 Coverage tracks were created with the Rscript from Ceto, createChIPtracks.R --extLen=150 to
603 extend reads to 150 bp, and coverage was normalized to total mapped reads (reads per million).
604 Peaks were called with MACS2 2.1.0 (Zhang et al. 2008) with a cutoff of -q 0.01 and the input
605 chromatin used as the control dataset. Heatmaps and composite plots were made with deepTools
606 (Ramirez et al. 2016) version 2.0. computeMatrix using reference-point peaks. “Black-listed”
607 regions were removed with parameter -bl Anshul_Hg19UltraHighSignalArtifactRegions.bed
608 (<ftp://encodeftp.cse.ucsc.edu/users/akundaje/rawdata/blacklists/hg19>). For metagene plots, we
609 used the Ensembl version 75 transcripts with the highest total coverage from the annotated TSS
610 to 200 nt downstream and were at least 2 kb long, and 1 kb away from the nearest gene.

611 *RNAi*. Lentiviruses were packaged in HEK293T cells transfected with 1 µg pME-VSVG,
612 2 µg PAX2 and 4 µg shRNA in pLKO.1 backbone using Lipofectamine 3000 (Thermo Fisher
613 Scientific, Waltham, MA) according to the manufacturer’s instructions. The virus particles were
614 then harvested 24 to 48 hours later by passing through a 0.45 µm syringe filter (Thermo
615 Scientific). Viruses were mixed with an equal volume of fresh media supplemented with 10%
616 FBS and polybrene was added at a final concentration of 5 µg/mL to increase infection

617 efficiency. The medium was changed 6 hours after infection. Cells were selected with 2 μ g/ml
618 puromycin for three days before Western blotting (anti-NRF1 rabbit mAb clone D9K6R from
619 CST and anti-beta tubulin mouse mAb clone E7 from DSHB) and ChIP-seq experiments. The
620 following shRNA sequences were used:

621

shNRF1-F2	CCGGCCTCATGTATTTGAGTCTAATCTCGAGATTAGACTCAAATACATGAGGTTTTTG
shNRF1-R2	AATTCAAAAACCTCATGTATTTGAGTCTAATCTCGAGATTAGACTCAAATACATGAGG
shNRF1-F3	CCGGCCGTTGCCCAAGTGAATTATTCTCGAGAATAATCACTGGGCAACGGTTTTTG
shNRF1-R3	AATTCAAAAACCGTTGCCCAAGTGAATTATTCTCGAGAATAATCACTGGGCAACGG

622

623 **Bioinformatic protocols**

624 *Technical performance.* A series of modular bioinformatic analyses were implemented to
625 evaluate technical success of ChIP-exo library construction and sequencing, independent of
626 whether the antibody found its target or not. 1) Sequencing depth (standard is 8-10M), which is
627 the total number of sequencing reads having a target-specific barcode. 2) Adapter dimers
628 (standard is <2%), which is the fraction of reads that contain the sequencing adapters but lack a
629 genomic insert. 3) Alignment (standard is 70-90%), which is the percent of reads that map to the
630 reference human genome after removing adapter dimers. 4) PCR duplicates (standard is <40%),
631 which are expected to have identically mapped Read_1 and Read_2 5' ends. We assume that
632 when Read_1 and Read_2 5' ends have identical mapped coordinates; they represent PCR
633 duplicates. Since Read_2 is generated by sonication it is expected to be distributed across a
634 region, and thus not likely to be at the same coordinate twice. Since PCR duplicates are not a
635 direct product of ChIP, they add no value to enrichment metrics. High PCR duplicates, at normal
636 sequencing depths, often means technical loss of material during library construction prior to
637 PCR.

638 *Peak calling.* We utilized two distinct algorithms for ChIP-exo peak-calling. The first
639 algorithm was GeneTrack which used a gaussian kernel to call strand-separated peaks at the 5'
640 ends of reads (Albert et al. 2008). The reads were then paired across strands and the tag
641 occupancy was normalized using the NCIS approach (Liang and Keles 2012). Peak significance
642 was called using either the binomial or Poisson test (taking whichever p-value was higher) with
643 Benjamini-Hochberg correction and a q-value cutoff of $q < 0.01$. GeneTrack was used to generate
644 the ChIP-exo peaks used in the manuscript figures. The other peak-caller used was the ChExMix
645 algorithm, which is a high-resolution peak-caller designed to simultaneously identify enriched
646 sequence motifs and distinct sub-types of binding using a combination of clustering and
647 hierarchical mixture modeling (Yamada et al. 2019). ChExMix was designed to take advantage
648 of ChIP-exo's ability to identify protein co-factors through indirect crosslinking events by
649 modeling detected tag distributions in ChIP-exo data and using tree-clustering based approaches
650 to determine the significant peak subtypes that exist with ChIP-exo data. ChExMix-called peaks
651 were used to interrogate the ChIP-exo peaks subtype structure and are visualized on the
652 www.PCRPvalidation.org website.

653 *Motif enrichment via ChExMix.* De novo motif discovery was performed by ChExMix.
654 Each motif was compared against the JASPAR database using TOMTOM with default
655 parameters to identify similarity to known motifs (Bailey et al. 2009; Fornes et al. 2020).
656 Heatmaps and composite plots were generated of sequence reads aligned relative to motif
657 midpoints of all peaks containing an enriched motif. For samples with high background, low
658 complexity, and/or low sequencing depth, it is possible the antibody is valid, but that standard de
659 novo motif discovery may fail. We developed an orthogonal method for motif detection. By first
660 identifying all non-redundant motif classes (Castro-Mondragon et al. 2017) in the genome, we
661 then overlap low-threshold ChExMix peaks and determined which motif class possesses
662 overlapping peaks above background ($>2 \log_2$).

663 *Motif enrichment and centering analysis.* For ChIP-exo data generated from K562,
664 HepG2 and MCF-7 cells, narrowpeak data were called using ChExMix (Yamada et al. 2019); we
665 restricted our motif enrichment analysis to narrowpeak datasets that contained more than 500
666 peaks. For ChIP-seq data generated from HCT116 cells, we required the presence of 100 peaks
667 due to the typical lower number of called peaks in those datasets as compared to ChIP-exo. Motif
668 enrichment analysis of ChIP-exo and ChIP-seq peaks was then performed as described
669 previously (Mariani et al. 2017). For ChIP-exo peaks, we first filtered for the datasets that had
670 more than 500 peaks, and then used for the comparison the top 500 peaks, with peaks defined as
671 the ChIP-exo summits computationally padded with the region spanning [-100 bp, +100 bp]. To
672 perform an analogous analysis on ChIP-seq peaks, we fixed both the number of peaks per dataset
673 (e.g., top 100 peaks) and the peak size, which we computationally trimmed similarly to the ChIP-
674 exo data to span [-100 bp, +100 bp] surrounding the ChIP-seq peak summit. For each ChIP peak
675 set, we generated background sequences using GENRE software with the default human setting,
676 to ensure the same level of promoter overlap, repeat overlap, GC content and CpG dinucleotide
677 frequency between each peak and its associated background sequence (Mariani et al. 2017). We
678 manually curated a collection of 100 position weight matrices (PWMs), primarily from
679 biochemical TF DNA binding assays (*i.e.*, PBM or HT-SELEX), from the UniPROBE and
680 CisBP databases, as a representative repertoire of human sequence-specific TF binding motifs
681 (Weirauch et al. 2014; Hume et al. 2015; Mariani 2020). We scored each sequence for matches
682 to each of the motifs using the function "matchPWM" from the "Biostrings" R package. Motif
683 enrichment was quantified using an established AUROC metric that assesses the presence of a
684 motif among the 500 highest confidence peaks (foreground set) as compared to the
685 corresponding background set of sequences using publicly available tools for analysis of TF
686 ChIP-seq data (Mariani et al. 2017). We also assessed each motif for its enrichment towards the
687 centers of each ChIP-exo or ChIP-Seq peak set as described previously (Mariani et al. 2017).
688 Briefly, we first identified the PWM score threshold that maximized the difference between
689 foreground and corresponding background sets in the number of sequences containing at least
690 one PWM match (*Optimal PWM Match Score*). If a sequence had multiple PWM matches, we
691 considered only the highest score site. We then calculated the distance from each of these sites to
692 the corresponding peak summits and used the mean of these distances in the foreground or
693 background set to quantify the motif enrichment towards the centers of ChIP peaks. The *P*-
694 values associated with motif enrichment (*i.e.*, AUROC value) and enrichment towards the peak

695 summits (*i.e.*, mean motif distance to peak summit) were both calculated by using a Wilcoxon
696 signed-rank test comparing their scores (PWM match score and PWM match distance to distance
697 to peak summit, respectively) for foreground and background sequences when the PWM
698 threshold was set to the optimal PWM match score. We then adjusted the *P*-values across the
699 PWM collection with a false discovery rate test for multiple hypothesis testing. To test the
700 significance of the difference in the TPM distributions between ChIP datasets with enriched
701 versus non-enriched motifs, we calculated the *P*-value by a Wilcoxon test using the function
702 `wilcox.test` in R.

703 *Genome annotation enrichment.* Only a small fraction of DNA-interacting factors binds
704 sequence-specific motifs. In the case of targets with either no expected motif or no known
705 function, determining peak enrichments at annotated regions of the genome can provide evidence
706 of ChIP success. The relative frequency of peaks occurring in different functional genomic
707 regions as defined by chromHMM was calculated for each target, an IgG negative control, and
708 for random expectation (Ernst et al. 2011). The \log_2 frequency enrichment of sample over IgG
709 control was used to identify regions of enrichment, as well as significant areas of de-enrichment
710 (regions that selectively avoid the target). Significant peaks were intersected with chromHMM
711 and Segway states to generate frequency histograms for overlap with predicted chromatin states
712 (Ernst et al. 2011; Hoffman et al. 2012). Peaks derived from the matched negative control dataset
713 were also intersected with annotated states. The \log_2 ratio of sample state frequency over control
714 state frequency was then calculated in order to identify general state enrichment of the sample
715 throughout the genome.

716 *Positional enrichment at promoters and insulators.* In order to identify enrichment in
717 well-characterized promoter regions, sequence reads for the target, a matched “No Antibody”
718 control, and an IgG were aligned relative to annotated transcription start sites (TSS). Heatmaps
719 of all genes and composite plots of the top 1,000 TSS by gene expression (RNA-seq FPKM)
720 were generated from the data⁷.

721 *Heatmaps, composite plots, and 4color sequence plots.* All heatmaps, composite plots,
722 and 4 color sequence plots were generated using ScriptManager v0.12
723 (<https://github.com/CEGRcode/scriptmanager>). ScriptManager is a Java-based GUI tool that
724 contains a series of interactive wizards that guide the user through transforming aligned BAM
725 files into publication-ready figures.

726

727 **CUT&RUN protocols**

728 *Antibody sourcing and concentration.* Antibody hybridoma supernatants, name, clone ID,
729 and lot) were from DSHB. mAbs were concentrated using Amicon Ultra-4 Centrifugal Filter
730 Units with a 50 kDa cut-off (Millipore Sigma Cat # UFC805024) following manufacturer’s
731 recommendations. All centrifugation steps (including 3x 4ml washes with 1X Tris buffered
732 Saline [TBS]) were performed at 4,000 x g for 15 minutes at room temperature. Final
733 concentrations for recovered mAbs (stored at 4°C in [TBS, 0.1% BSA, 0.09% Sodium Azide])
734 were assumed based on initial concentrations / final recovery volumes and 1 μ g used per
735 CUT&RUN experiment.

736 *CUT&RUN*. CUT&RUN was performed on 500k native nuclei extracted from K562 cells
737 using CUTANA[®] protocol v1.5.1 [<http://www.epicypher.com>] which is an optimized version of
738 that previously described (Skene et al. 2018). For each sample, nuclei were extracted by
739 incubating cells on ice for 10 min in Nuclei Extraction buffer (NE: 20 mM HEPES–KOH, pH
740 7.9; 10 mM KCl; 0.1% Triton X-100; 20% Glycerol; 0.5mM spermidine; 1x complete protease
741 inhibitor [*Roche* # 11836170001]), collecting by centrifugation (600 g, 3 min, 4°C), discarding
742 the supernatant, and resuspending at [100 µl / 500K nuclei] sample in NE buffer. For each target
743 500K nuclei were immobilized onto Concanavalin-A beads (*EpiCypher* #21-1401) and incubated
744 overnight (4°C with gentle rocking) with 1 µg of antibody (For all 40 PCR antibodies as above;
745 RbIgG (*EpiCypher* 13-0042, lot 20036001-52); MsIgG (Invitrogen 10400C, lot VD293456);
746 CTCF (*Millipore* 07-729, lot 3205452).

747 *Modified CUT&RUN library prep*. Illumina sequencing libraries were prepared from 1ng
748 to 10ng of purified CUT&RUN DNA using NEBNext Ultra II DNA Library Prep Kit (*New*
749 *England Biolabs* # E7645) as previously (Liu et al. 2018) with the following modifications to
750 preserve and enrich smaller DNA fragments (20-70 bp). Briefly, during end repair the cycling
751 time was decreased to 30 mins at 50°C. After adapter ligation, to purify fragments >50bp, 1.75x
752 volumes of Agencourt AMPure XP beads (*Beckman Coulter* #A63881) were added for the first
753 bead clean-up before amplification following manufacturer's recommendations. PCR
754 amplification cycling parameters were as described (Skene et al. 2018). Post-PCR, two rounds of
755 DNA size selection were performed. For the first selection, 0.8x volume of AMPure XP beads
756 was added to the PCR reaction to remove products >350bp. The supernatant, containing
757 fragments <350bp, was moved forward to a second round of size selection using 1.2x volumes of
758 AMPure XP beads, to remove products <150 bp. Libraries were quantified using Qubit
759 Fluorometer (*Invitrogen*) and checked for size distribution with a Bioanalyzer (*Agilent*).

760 *CUT&RUN library sequencing and data analysis*. Libraries were sequenced on the
761 *Illumina* NextSeq 550, obtaining ~5 million paired-end reads (75 x 75 nucleotides) on average.
762 Paired-end FASTQ files were aligned to the hg19 reference genome using the ChIP-exo pipeline.
763

764 **TF cloning, protein expression, western blots, and PBM protocols**

765 Full-length TFs were either obtained from the hORFeome clone collection or synthesized
766 as gBlocks (Integrated DNA Technologies) (**Supplementary Table 7**), full-length sequence-
767 verified, and transferred by Gateway recombinational cloning into either the pDEST15
768 (ThermoFisher Scientific) or pT7CFE1-NHIS-GST (ThermoFisher) vectors for expression as N-
769 terminal GST fusion proteins (Collaboration 2016). TFs were expressed by a coupled *in vitro*
770 transcription and translation kit according to the manufacturer's protocols (**Supplementary**
771 **Table 6**). Protein concentrations were approximated by an anti-GST western blot as described
772 previously (Berger et al. 2006). All PCR antibodies were used at a final concentration of 40
773 ng/mL in western blots; based on successful outcomes in PBM experiments, PCR antibodies
774 1A7 (anti-GATA4), 2A4 (anti-HNF4A), and 1B3 (anti-PAX3) were also used at a final
775 concentration of 1,000 ng/mL in western blots. 8x60K GSE 'all 10-mer universal'
776 oligonucleotide arrays (AMADID #030236; Agilent Technologies, Inc.) were double-stranded
777 and used in PBM experiments essentially as described previously, with minor modifications as
778 described below (Berger et al. 2006; Berger and Bulyk 2009; Nakagawa et al. 2013). GST-

779 tagged TFs assayed in PBMs were detected either with Alexa488-conjugated anti-GST antibody
780 (Invitrogen A-11131), or with a TF-specific PCRPs antibody, followed by washes and detection
781 with Alexa488-conjugated goat anti-mouse IgG(H+L) Cross-Adsorbed Secondary Antibody
782 (Invitrogen A-11001), essentially as described previously (Siggers et al. 2011b) (**Supplementary**
783 **Table 6**). All PCRPs Abs were used undiluted in PBM experiments; a subset of the PCRPs Abs
784 were also tested at a 1:5 or 1:20 dilution (**Supplementary Table 6**). All PBM experiments using
785 PCRPs antibodies were performed using fresh arrays or arrays that had been stripped once, as
786 described previously (Berger et al. 2006; Berger and Bulyk 2009). PBMs were scanned in a
787 GenePix 4400A Microarray Scanner and raw data files were quantified and processed using the
788 Universal PBM Analysis Suite (Berger et al. 2006; Berger and Bulyk 2009).

789

790 **STORM protocols**

791 *Supernatant concentration.* 3 milliliters of PCRPs supernatant were concentrated using the
792 Amicon® Pro Affinity Concentration Kit Protein G with 10kDa Amicon® Ultra-0.5 Device
793 following the manufacturer's recommendations. Supernatant was quantitated by
794 spectrophotometer for rough approximation of concentration.

795 *Cellular preparation and staining.* K562 cells obtained from the ATCC (cat number
796 CCL243) were grown in a humidified 5% CO₂ incubator. 3-5x10⁵ cells were centrifuged at
797 1,500 rpm for 5 minutes, washed with PBS, and plated on MatTek-brand glass bottom dishes
798 (P35-G.1) prepared appropriately (washes with increasing concentrations of ethanol, followed by
799 coating with poly-L-Lysine (Sigma P4707) for 5 minutes and subsequent washes with water and
800 air-drying for 2h.) After plating, the cells were allowed to adhere for 2h and then washed with
801 PBS. For fixation, 1ml of 4% paraformaldehyde and 0.1% glutaraldehyde in PBS were added
802 for 10 minutes at room temperature with gentle rocking followed by blocking and
803 permeabilization in 2% normal goat serum/1% Triton X-100 in PBS for 1h at room temperature
804 with gentle shaking. Immunostaining was performed with anti-MTR4 antibody (Abcam 70551)
805 at a dilution of 1:250 in 0.1% normal goat serum, 0.05% Triton X-100 overnight at 4 degrees C.
806 The next morning cells were incubated with the secondary antibody (conjugated to Alexa-Fluor
807 647 (Life Technologies)) at a 1:1000 dilution in 0.1% normal goat serum in PBS and incubated
808 for 2h at room temperature followed by washes in PBS. This material was then subjected to
809 immunostaining with PCRPs antibodies, by repeating the above procedure. PCRPs mAb
810 hybridoma supernatant (3 ml) was first concentrated 30-100 fold since raw supernatants were
811 unsuccessful in both confocal microscopy and STORM (data not shown). The secondary
812 antibody was conjugated to Alexa-Fluor 488 (Life Technologies). At the end of the application
813 of the second secondary antibody, the cells were washed 3x with PBS and DAPI (Sigma D8542)
814 at a concentration of 1:500 in 0.1% normal goat serum in 1x PBS was applied for 10 minutes at
815 room temperature. The cells were washed 3x with PBS and finally 4% paraformaldehyde/0.1%
816 glutaraldehyde in PBS was applied for 10 minutes at RT before 3 washes in 1x PBS were
817 performed and dishes stored at 4 degrees until microscopy could be performed.

818 *Microscopy.* Cells were brought to the imaging facility and OXEA buffer was applied (50
819 mM Cysteimine, 3% v/v Oxyfluor, 20% v/v sodium DL Lactate, with pH adjusted to
820 approximately 8.5, as necessary.) The two colors (Alexa fluor 488 and Alexa fluor 647) were
821 imaged sequentially. Imaging buffer helped to keep dye molecules in a transient dark state.

822 Subsequently, individual dye molecules were excited stochastically with high laser power at their
823 excitation wavelength (488 nm for Alexa fluor 488 or 647 nm for Alexa fluor 647, respectively)
824 to induce blinking on millisecond timescales. STORM images and the correlated high-power
825 confocal stacks were acquired via a CFI Apo TIRF 100 × objective (1.49 NA) on a Nikon Ti-E
826 inverted microscope equipped with a Nikon N-STORM system, an Agilent laser launch system,
827 an Andor iXon Ultra 897 EMCCD (with a cylindrical lens for astigmatic 3D-STORM imaging)
828 camera, and an NSTORM Quad cube (Chroma). This setup was controlled by Nikon NIS-
829 Element AR software with N-STORM module. To obtain images, the field of view was selected
830 based on the live EMCCD image under 488-nm illumination. 3D STORM datasets of 50,000
831 frames were collected. Lateral drift between frames was corrected by tracking 488, 561, and 647
832 fluorescent beads (TetraSpeck, Life Technologies). STORM images were processed to acquire
833 coordinates of localization points using the N-STORM module in NIS-Elements AR software.
834 Identical settings were used for every image. Each localization is depicted in the STORM image
835 as a Gaussian peak, the width of which is determined by the number of photons detected (Betzig
836 et al. 2006). All of the 3D STORM imaging was performed on a minimum of two different K562
837 cells.

838

839 **Code Availability**

840 Our automated bioinformatic ChIP-exo analysis pipeline can be found at
841 (<https://github.com/CEGRcode/PCRPpipeline>).

842

843 **Data Availability**

844 Raw ChIP-exo sequencing files are available at NCBI GEO archive (GSE151287). Raw ChIP-
845 seq sequencing files are available at NCBI GEO archive (GSE152144). PBM data will be
846 available via the UniPROBE database (accession ID: LAI20A) upon publication. CUT&RUN
847 data has been deposited at GEO: Accession GSE151326 [(5.27.20) NCBI tracking system
848 #20907832]. Peak files for all figures are available at ([https://github.com/CEGRcode/2021-
849 Lai_PCRP](https://github.com/CEGRcode/2021-Lai_PCRP))

850

851 **Acknowledgements**

852 The Basu lab would like to thank Drs. Teresa Swayne and Emilia Laura Munteanu of the Herbert
853 Irving Comprehensive Cancer Center Core Microscopy facility at Columbia University. The
854 Pugh lab would like to thank Kyle Nilson for donating the peroxide stressed cells. The
855 Shilatifard lab would like to thank Anna Whelan and Jordan Harris for technical assistance and
856 Zibo Zhao and Marc Morgan for helpful discussions. The Bulyk lab thanks Steve S. Gisselbrecht
857 for assistance with preparation of figures. ChIP-exo data was made available through the Cornell
858 Institute of Biotechnology's Epigenomic Core Facility using the Platform for Epigenome and
859 Genomic Research (PEGR), with NIH 5R01-ES013768-12 funding for the development and
860 dissemination of PEGR. The authors gratefully acknowledge the support of the Institute for
861 Computational and Data Sciences at the Pennsylvania State University through an ICDS Seed
862 Grant. This work was supported by an administrative supplement to NIAID grant
863 1R01AI099195 to U.B., an administrative supplement to NIH grant R21 HG009268 to M.L.B.,

864 an administrative supplement to NIH grant R01-ES013768 to B.F.P., an administrative
865 supplement to NIH grant R01CA214035 to A.S., NIH grant R50CA211428 to E.R.S., and NIH
866 grant R44 DE029633 to EpiCypher.

867

868

869 **Author Contributions**

870 In the Basu lab, G.R. performed STORM experiments; W.Z. performed required bioinformatics
871 analyses of STORM data; U.B. analyzed data, provided oversight and co-wrote the manuscript.
872 In the Bulyk lab, J.T.A. and S.K.P. performed cloning, protein expression, western blots, PBM
873 experiments, and PBM analysis; L.M. performed analysis of motif enrichment and centering;
874 S.K.P. and L.M. prepared figures and Supplementary Tables; M.L.B. supervised research; and
875 S.K.P., L.M., and M.L.B. co-wrote the manuscript. In the Pugh lab, TRB, KB, JM, SND, and
876 KM performed ChIP-exo assays. PK designed and implemented the web portal. MJR and DJ
877 performed ChIP-exo library quantitation and sequencing. WKML directed the ChIP-exo
878 experiments, processed and analyzed the ChIP-exo, and co-wrote the manuscript writing. BFP
879 provided oversight for ChIP-exo and co-wrote the manuscript. In the Shilatifard lab, A.P.S.
880 conducted experiments. E.R.S. analyzed ChIP-seq data. E.R.S. and A.S. provided oversight and
881 co-wrote the manuscript. From EpiCypher, B.J.V., K.N. and E.M. performed CUT&RUN
882 studies, and M-C.K. provided oversight and co-wrote the manuscript.

883

884 **Competing Interests**

885 M.L.B. is a co-inventor on U.S. patent #8,530,638 on universal PBM technology. BFP has a
886 financial interest in Peconic, LLC, which utilizes the ChIP-exo technology implemented in this
887 study and could potentially benefit from the outcomes of this research. EpiCypher is a
888 commercial developer of reagents to support CUTANA[®] CUT&RUN. The authors in the Basu
889 and Shilatifard labs declare no competing financial interests.

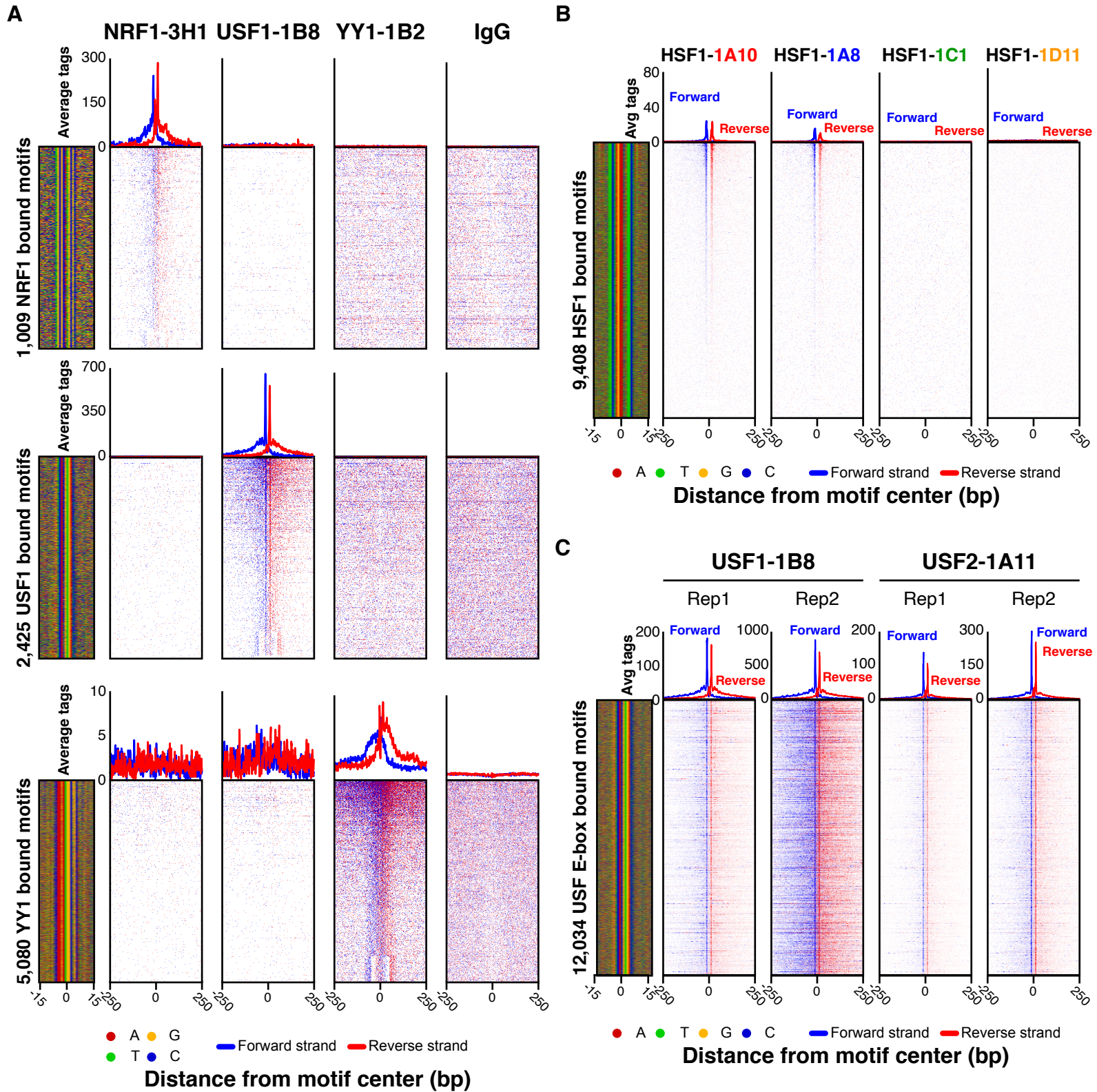
890 **REFERENCES**

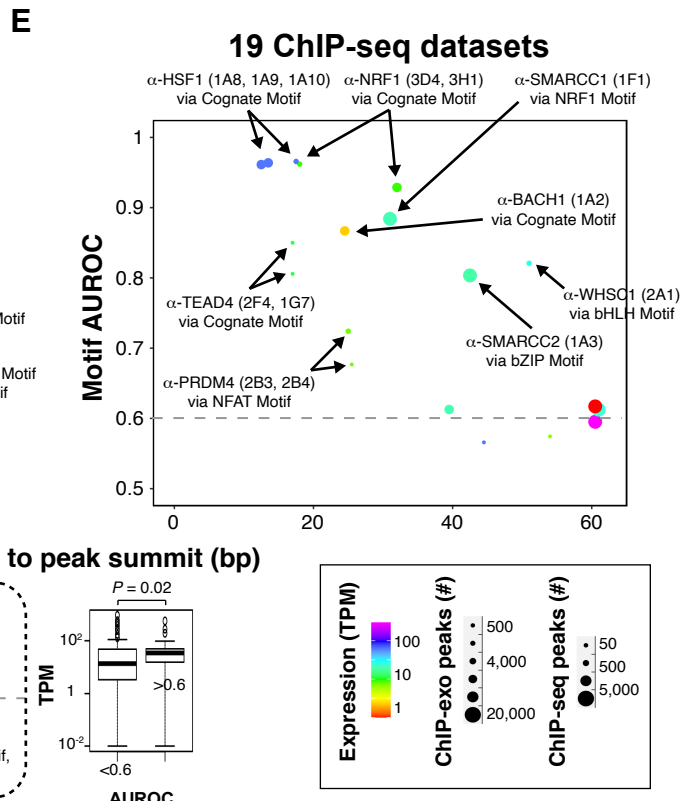
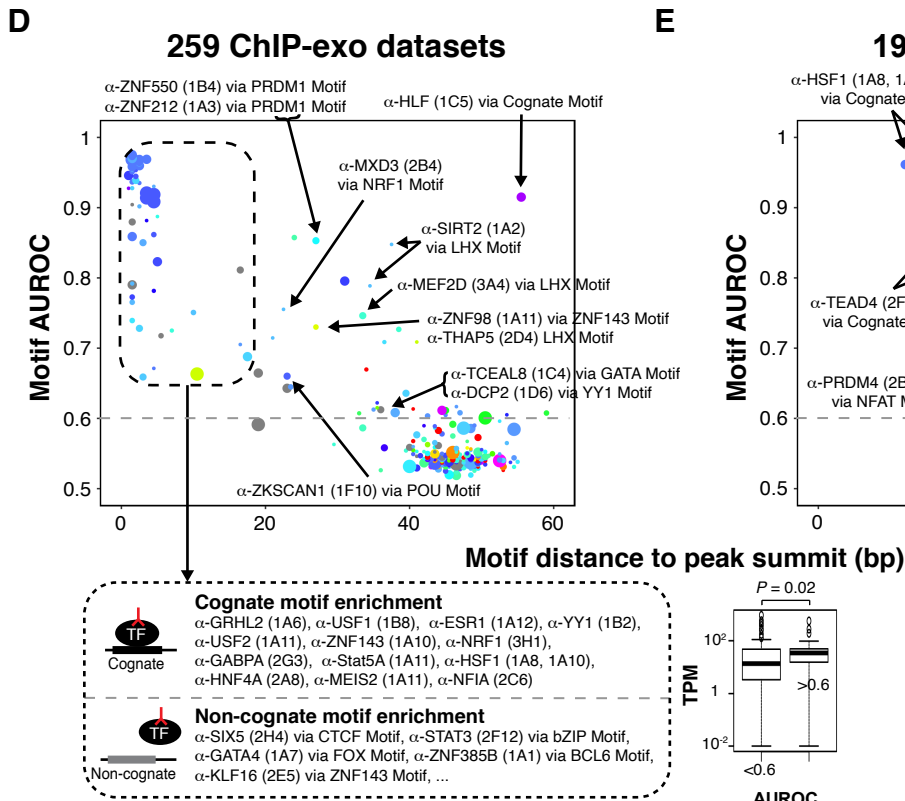
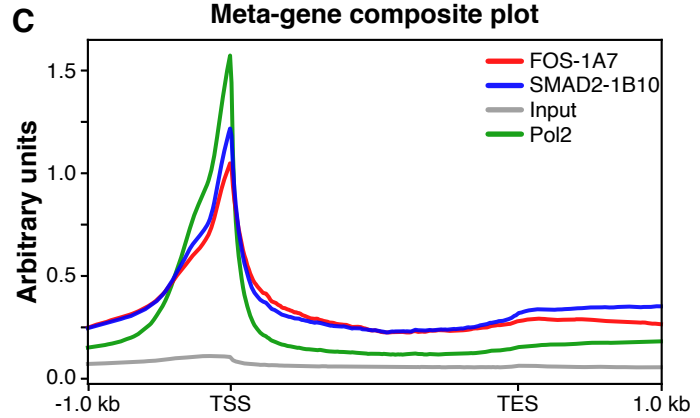
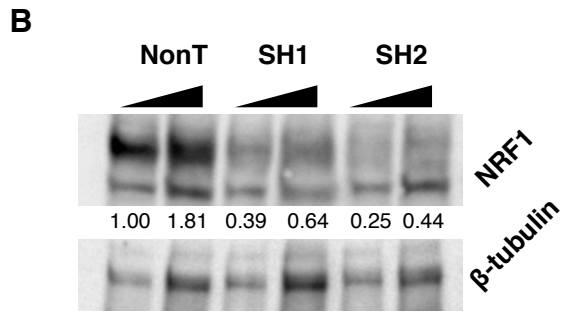
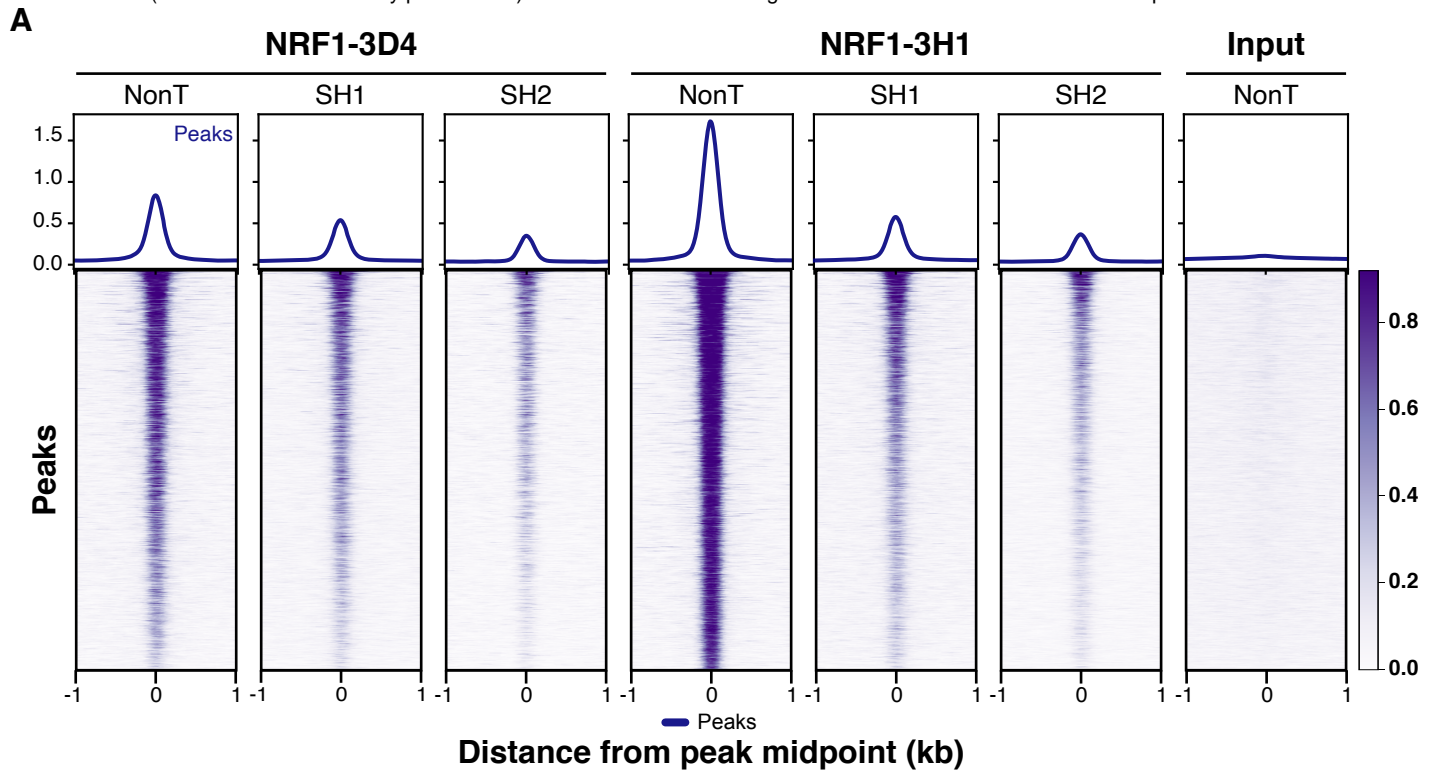
- 891 Albert I, Wachi S, Jiang C, Pugh BF. 2008. GeneTrack--a genomic data processing and
892 visualization framework. *Bioinformatics* **24**: 1305-1306.
- 893 Aragon E, Wang Q, Zou Y, Morgani SM, Ruiz L, Kaczmarek Z, Su J, Torner C, Tian L, Hu J et
894 al. 2019. Structural basis for distinct roles of SMAD2 and SMAD3 in FOXH1 pioneer-
895 directed TGF-beta signaling. *Genes Dev* **33**: 1506-1524.
- 896 Bailey TL, Boden M, Buske FA, Frith M, Grant CE, Clementi L, Ren J, Li WW, Noble WS.
897 2009. MEME SUITE: tools for motif discovery and searching. *Nucleic Acids Res* **37**:
898 W202-208.
- 899 Bailey TL, Machanick P. 2012. Inferring direct DNA binding from ChIP-seq. *Nucleic Acids Res*
900 **40**: e128.
- 901 Baker M. 2015. Reproducibility crisis: Blame it on the antibodies. *Nature* **521**: 274-276.
- 902 Baler R, Dahl G, Voellmy R. 1993. Activation of human heat shock genes is accompanied by
903 oligomerization, modification, and rapid translocation of heat shock transcription factor
904 HSF1. *Mol Cell Biol* **13**: 2486-2496.
- 905 Berger MF, Bulyk ML. 2009. Universal protein-binding microarrays for the comprehensive
906 characterization of the DNA-binding specificities of transcription factors. *Nat Protoc* **4**:
907 393-411.
- 908 Berger MF, Philippakis AA, Qureshi AM, He FS, Estep PW, 3rd, Bulyk ML. 2006. Compact,
909 universal DNA microarrays to comprehensively determine transcription-factor binding
910 site specificities. *Nat Biotechnol* **24**: 1429-1435.
- 911 Betzig E, Patterson GH, Sougrat R, Lindwasser OW, Olenych S, Bonifacino JS, Davidson MW,
912 Lippincott-Schwartz J, Hess HF. 2006. Imaging intracellular fluorescent proteins at
913 nanometer resolution. *Science* **313**: 1642-1645.
- 914 Blackshaw S, Venkataraman A, Irizarry J, Yang K, Anderson S, Campbell E, Gatlin CL,
915 Freeman NL, Basavappa R, Stewart R et al. 2016. The NIH Protein Capture Reagents
916 Program (PCRP): a standardized protein affinity reagent toolbox. *Nat Methods* **13**: 805-
917 806.
- 918 Castro-Mondragon JA, Jaeger S, Thieffry D, Thomas-Chollier M, van Helden J. 2017. RSAT
919 matrix-clustering: dynamic exploration and redundancy reduction of transcription factor
920 binding motif collections. *Nucleic Acids Res* **45**: e119.
- 921 Chames P, Van Regenmortel M, Weiss E, Baty D. 2009. Therapeutic antibodies: successes,
922 limitations and hopes for the future. *Br J Pharmacol* **157**: 220-233.
- 923 Collaboration OR. 2016. The ORFeome Collaboration: a genome-scale human ORF-clone
924 resource. *Nat Methods* **13**: 191-192.
- 925 Consortium TEP. 2012. An integrated encyclopedia of DNA elements in the human genome.
926 *Nature* **489**: 57-74.
- 927 Edfors F, Hober A, Linderback K, Maddalo G, Azimi A, Sivertsson A, Tegel H, Hober S,
928 Szigartyo CA, Fagerberg L et al. 2018. Enhanced validation of antibodies for research
929 applications. *Nat Commun* **9**: 4130.
- 930 Egelhofer TA, Minoda A, Klugman S, Lee K, Kolasinska-Zwierz P, Alekseyenko AA, Cheung
931 MS, Day DS, Gadel S, Gorchakov AA et al. 2011. An assessment of histone-modification
932 antibody quality. *Nat Struct Mol Biol* **18**: 91-93.
- 933 Engelen E, Brandsma JH, Moen MJ, Signorile L, Dekkers DH, Demmers J, Kockx CE, Ozgur Z,
934 van IWF, van den Berg DL et al. 2015. Proteins that bind regulatory regions identified by
935 histone modification chromatin immunoprecipitations and mass spectrometry. *Nat*
936 *Commun* **6**: 7155.

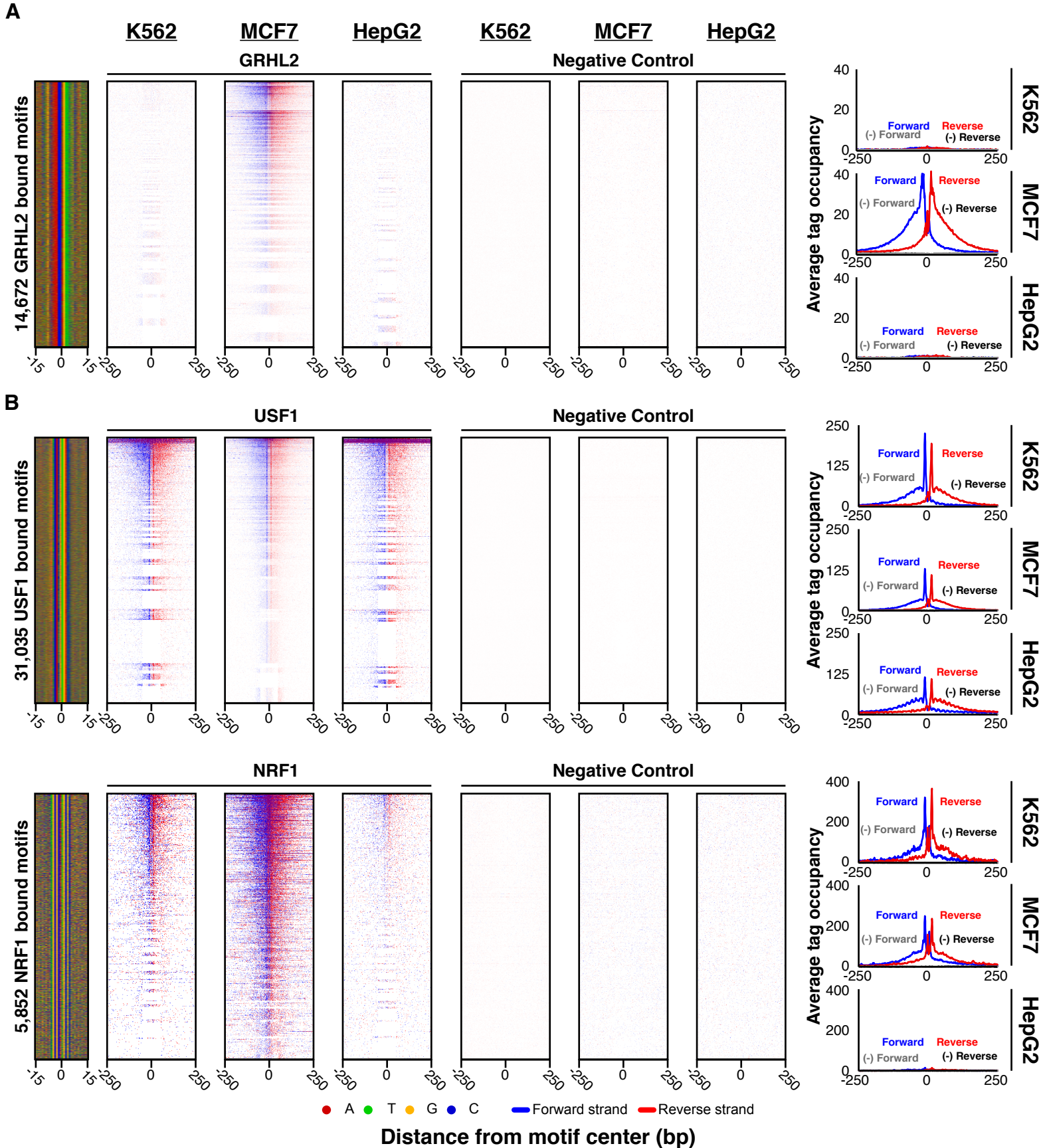
- 937 Ernst J, Kheradpour P, Mikkelsen TS, Shoresh N, Ward LD, Epstein CB, Zhang X, Wang L,
938 Issner R, Coyne M et al. 2011. Mapping and analysis of chromatin state dynamics in nine
939 human cell types. *Nature* **473**: 43-49.
- 940 Fornes O, Castro-Mondragon JA, Khan A, van der Lee R, Zhang X, Richmond PA, Modi BP,
941 Correard S, Gheorghe M, Baranasic D et al. 2020. JASPAR 2020: update of the open-
942 access database of transcription factor binding profiles. *Nucleic Acids Res* **48**: D87-D92.
- 943 Gordan R, Hartemink AJ, Bulyk ML. 2009. Distinguishing direct versus indirect transcription
944 factor-DNA interactions. *Genome Res* **19**: 2090-2100.
- 945 Gupta S, Stamatoyannopoulos JA, Bailey TL, Noble WS. 2007. Quantifying similarity between
946 motifs. *Genome Biol* **8**: R24.
- 947 Hanly WC, Artwohl JE, Bennett BT. 1995. Review of Polyclonal Antibody Production
948 Procedures in Mammals and Poultry. *ILAR J* **37**: 93-118.
- 949 Hoffman MM, Buske OJ, Wang J, Weng Z, Bilmes JA, Noble WS. 2012. Unsupervised pattern
950 discovery in human chromatin structure through genomic segmentation. *Nat Methods* **9**:
951 473-476.
- 952 Hoffman MM, Ernst J, Wilder SP, Kundaje A, Harris RS, Libbrecht M, Giardine B, Ellenbogen
953 PM, Bilmes JA, Birney E et al. 2013. Integrative annotation of chromatin elements from
954 ENCODE data. *Nucleic Acids Res* **41**: 827-841.
- 955 Hume MA, Barrera LA, Gisselbrecht SS, Bulyk ML. 2015. UniPROBE, update 2015: new tools
956 and content for the online database of protein-binding microarray data on protein-DNA
957 interactions. *Nucleic Acids Res* **43**: D117-122.
- 958 Kohler G, Milstein C. 1975. Continuous cultures of fused cells secreting antibody of predefined
959 specificity. *Nature* **256**: 495-497.
- 960 Landt SG, Marinov GK, Kundaje A, Kheradpour P, Pauli F, Batzoglou S, Bernstein BE, Bickel
961 P, Brown JB, Cayting P et al. 2012. ChIP-seq guidelines and practices of the ENCODE
962 and modENCODE consortia. *Genome Res* **22**: 1813-1831.
- 963 Langmead B, Trapnell C, Pop M, Salzberg SL. 2009. Ultrafast and memory-efficient alignment
964 of short DNA sequences to the human genome. *Genome Biol* **10**: R25.
- 965 Lee TI, Johnstone SE, Young RA. 2006. Chromatin immunoprecipitation and microarray-based
966 analysis of protein location. *Nat Protoc* **1**: 729-748.
- 967 Liang K, Keles S. 2012. Normalization of ChIP-seq data with control. *BMC Bioinformatics* **13**:
968 199.
- 969 Lim J, Giri PK, Kazadi D, Laffleur B, Zhang W, Grinstein V, Pefanis E, Brown LM, Ladewig E,
970 Martin O et al. 2017. Nuclear Proximity of Mtr4 to RNA Exosome Restricts DNA
971 Mutational Asymmetry. *Cell* **169**: 523-537 e515.
- 972 Lin JR, Fallahi-Sichani M, Sorger PK. 2015. Highly multiplexed imaging of single cells using a
973 high-throughput cyclic immunofluorescence method. *Nat Commun* **6**: 8390.
- 974 Liu JK. 2014. The history of monoclonal antibody development - Progress, remaining challenges
975 and future innovations. *Ann Med Surg (Lond)* **3**: 113-116.
- 976 Liu N, Hargreaves VV, Zhu Q, Kurland JV, Hong J, Kim W, Sher F, Macias-Trevino C, Rogers
977 JM, Kurita R et al. 2018. Direct Promoter Repression by BCL11A Controls the Fetal to
978 Adult Hemoglobin Switch. *Cell* **173**: 430-442 e417.
- 979 Mahmood T, Yang PC. 2012. Western blot: technique, theory, and trouble shooting. *N Am J Med*
980 *Sci* **4**: 429-434.
- 981 Mariani L, Weinand K, Vedenko A, Barrera LA, Bulyk ML. 2017. Identification of Human
982 Lineage-Specific Transcriptional Coregulators Enabled by a Glossary of Binding
983 Modules and Tunable Genomic Backgrounds. *Cell Syst* **5**: 187-201 e187.

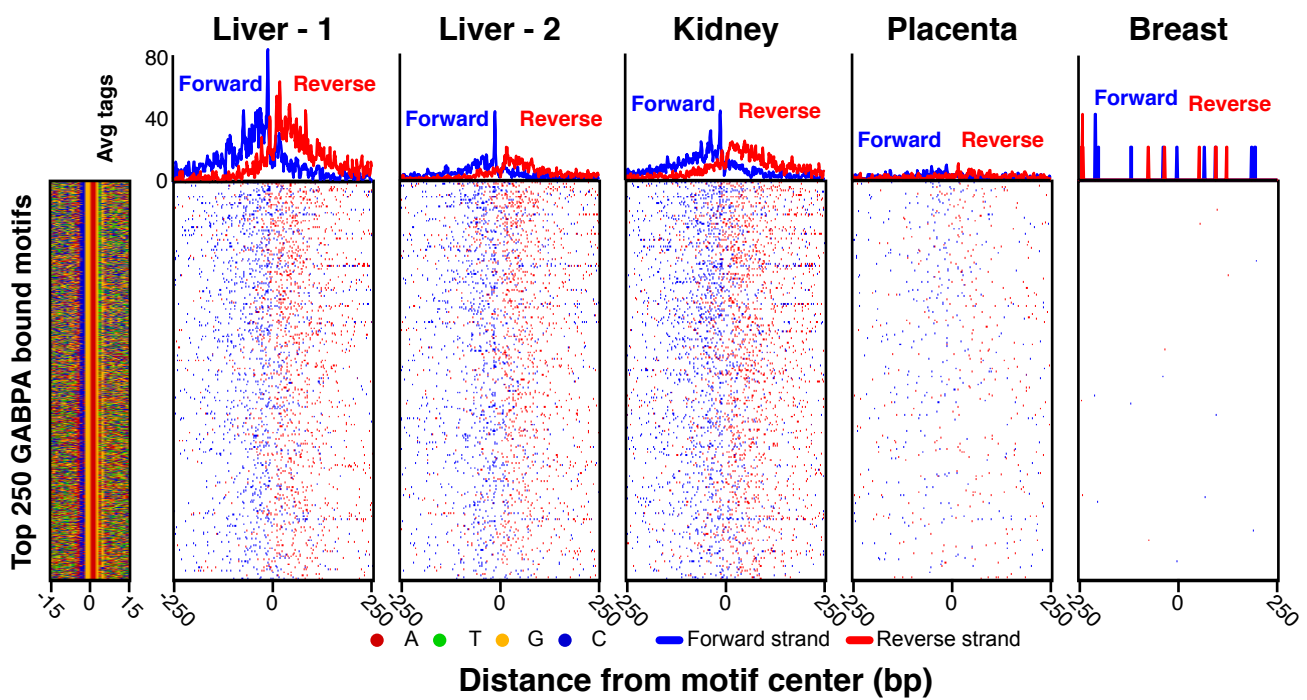
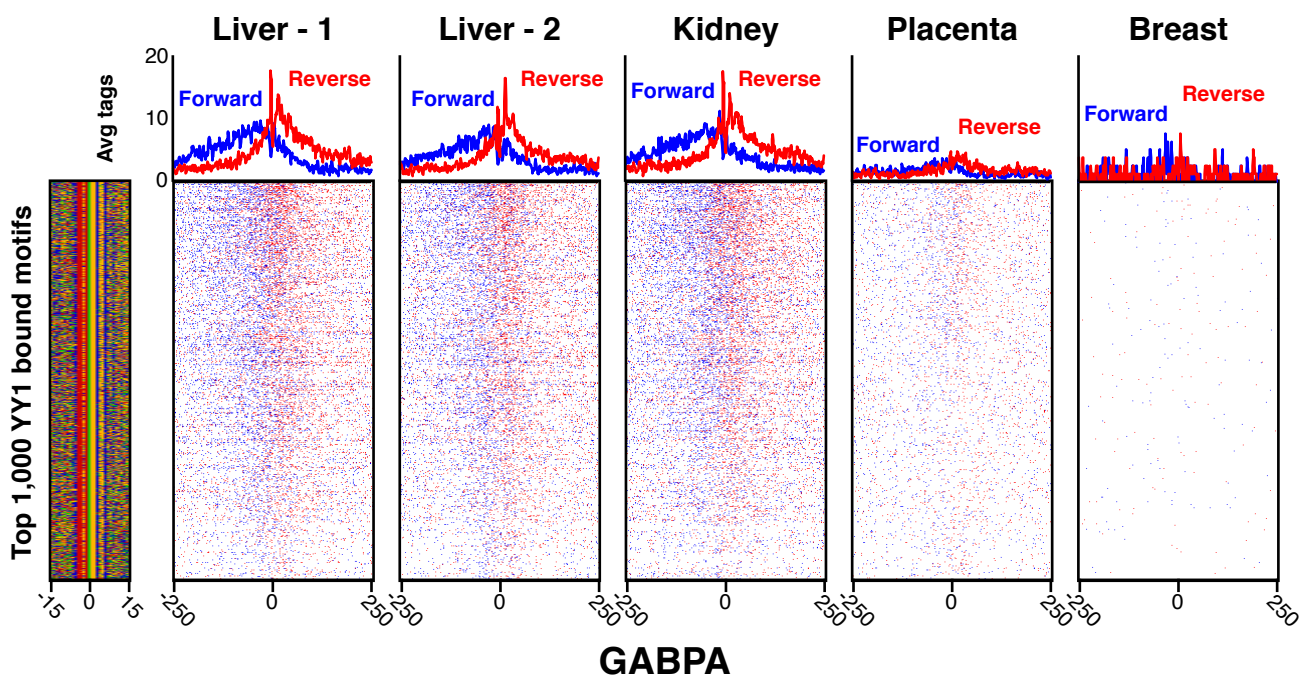
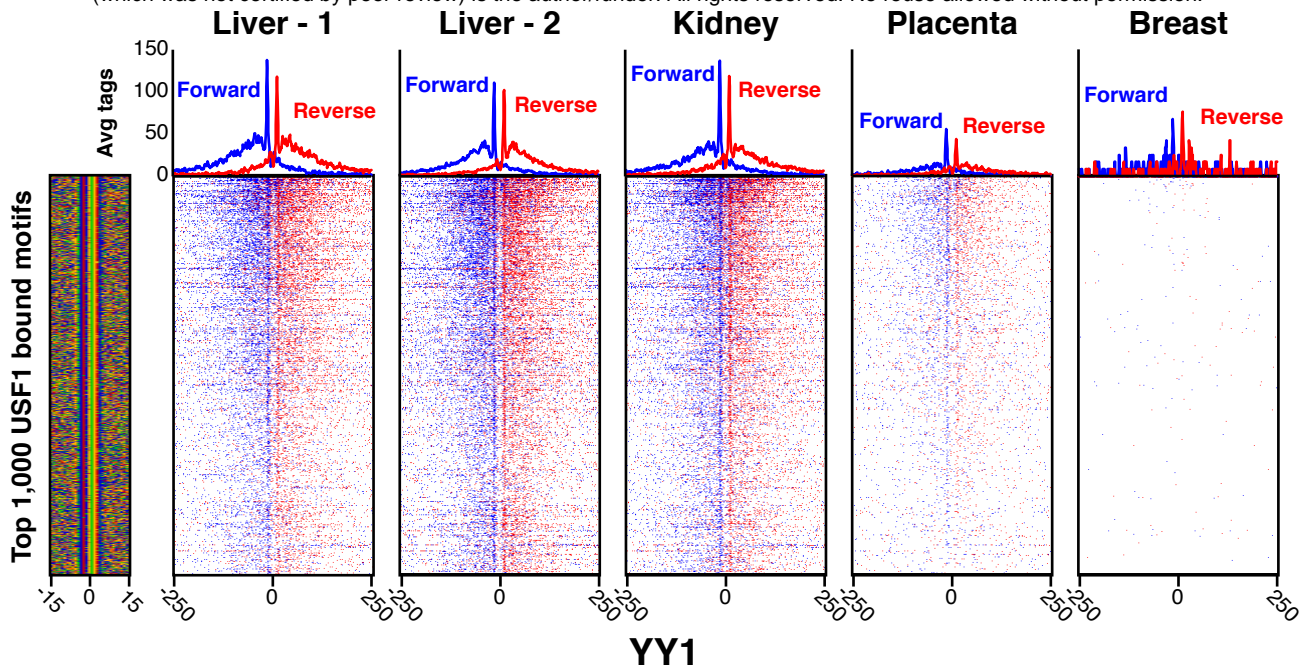
- 984 Mariani L, Weinand, K., Gisselbrecht, S.S. & Bulyk, M.L. 2020. MEDEA: Analysis of
985 Transcription Factor Binding Motifs in Accessible Chromatin. *Genome Res In Press*.
- 986 Marx V. 2019. What to do about those immunoprecipitation blues. *Nat Methods* **16**: 289-292.
- 987 Mukherjee S, Berger MF, Jona G, Wang XS, Muzzey D, Snyder M, Young RA, Bulyk ML.
988 2004. Rapid analysis of the DNA-binding specificities of transcription factors with DNA
989 microarrays. *Nat Genet* **36**: 1331-1339.
- 990 Nakagawa S, Gisselbrecht SS, Rogers JM, Hartl DL, Bulyk ML. 2013. DNA-binding specificity
991 changes in the evolution of forkhead transcription factors. *Proc Natl Acad Sci U S A* **110**:
992 12349-12354.
- 993 Park PJ. 2009. ChIP-seq: advantages and challenges of a maturing technology. *Nat Rev Genet*
994 **10**: 669-680.
- 995 Rada-Iglesias A, Ameer A, Kapranov P, Enroth S, Komorowski J, Gingeras TR, Wadelius C.
996 2008. Whole-genome maps of USF1 and USF2 binding and histone H3 acetylation reveal
997 new aspects of promoter structure and candidate genes for common human disorders.
998 *Genome Res* **18**: 380-392.
- 999 Ramirez F, Ryan DP, Gruning B, Bhardwaj V, Kilpert F, Richter AS, Heyne S, Dundar F,
1000 Manke T. 2016. deepTools2: a next generation web server for deep-sequencing data
1001 analysis. *Nucleic Acids Res* **44**: W160-165.
- 1002 Reardon S. 2016. Thousands of goats and rabbits vanish from major biotech lab. In *Nature*.
- 1003 Rhee HS, Pugh BF. 2011. Comprehensive genome-wide protein-DNA interactions detected at
1004 single-nucleotide resolution. *Cell* **147**: 1408-1419.
- 1005 Rhee HS, Pugh BF. 2012. ChIP-exo method for identifying genomic location of DNA-binding
1006 proteins with near-single-nucleotide accuracy. *Curr Protoc Mol Biol* **Chapter 21**: Unit
1007 21 24.
- 1008 Roadmap Epigenomics C, Kundaje A, Meuleman W, Ernst J, Bilenky M, Yen A, Heravi-
1009 Moussavi A, Kheradpour P, Zhang Z, Wang J et al. 2015. Integrative analysis of 111
1010 reference human epigenomes. *Nature* **518**: 317-330.
- 1011 Rohs R, West SM, Sosinsky A, Liu P, Mann RS, Honig B. 2009. The role of DNA shape in
1012 protein-DNA recognition. *Nature* **461**: 1248-1253.
- 1013 Rossi MJ, Lai WKM, Pugh BF. 2018. Simplified ChIP-exo assays. *Nat Commun* **9**: 2842.
- 1014 Shah RN, Grzybowski AT, Cornett EM, Johnstone AL, Dickson BM, Boone BA, Cheek MA,
1015 Cowles MW, Maryanski D, Meiners MJ et al. 2018. Examining the Roles of H3K4
1016 Methylation States with Systematically Characterized Antibodies. *Mol Cell* **72**: 162-177
1017 e167.
- 1018 Siggers T, Chang AB, Teixeira A, Wong D, Williams KJ, Ahmed B, Ragoussis J, Udalova IA,
1019 Smale ST, Bulyk ML. 2011a. Principles of dimer-specific gene regulation revealed by a
1020 comprehensive characterization of NF-kappaB family DNA binding. *Nat Immunol* **13**:
1021 95-102.
- 1022 Siggers T, Duyzend MH, Reddy J, Khan S, Bulyk ML. 2011b. Non-DNA-binding cofactors
1023 enhance DNA-binding specificity of a transcriptional regulatory complex. *Mol Syst Biol*
1024 **7**: 555.
- 1025 Sikorski K, Mehta A, Inngjerdigen M, Thakor F, Kling S, Kalina T, Nyman TA, Stensland ME,
1026 Zhou W, de Souza GA et al. 2018. A high-throughput pipeline for validation of
1027 antibodies. *Nat Methods* **15**: 909-912.
- 1028 Skene PJ, Henikoff JG, Henikoff S. 2018. Targeted in situ genome-wide profiling with high
1029 efficiency for low cell numbers. *Nat Protoc* **13**: 1006-1019.
- 1030 Son KK, Tkach D, Rosenblatt J. 2001. Delipidated serum abolishes the inhibitory effect of serum
1031 on in vitro liposome-mediated transfection. *Biochim Biophys Acta* **1511**: 201-205.

- 1032 Su J, Morgani SM, David CJ, Wang Q, Er EE, Huang YH, Basnet H, Zou Y, Shu W, Soni RK et
1033 al. 2020. TGF-beta orchestrates fibrogenic and developmental EMTs via the RAS
1034 effector RREB1. *Nature* **577**: 566-571.
- 1035 Trescher S, Leser U. 2019. Estimation of Transcription Factor Activity in Knockdown Studies.
1036 *Sci Rep* **9**: 9593.
- 1037 Uhlen M, Bandrowski A, Carr S, Edwards A, Ellenberg J, Lundberg E, Rimm DL, Rodriguez H,
1038 Hiltke T, Snyder M et al. 2016. A proposal for validation of antibodies. *Nat Methods* **13**:
1039 823-827.
- 1040 Uhlen M, Bjorling E, Agaton C, Szigyarto CA, Amini B, Andersen E, Andersson AC, Angelidou
1041 P, Asplund A, Asplund C et al. 2005. A human protein atlas for normal and cancer tissues
1042 based on antibody proteomics. *Mol Cell Proteomics* **4**: 1920-1932.
- 1043 Venkataraman A, Yang K, Irizarry J, Mackiewicz M, Mita P, Kuang Z, Xue L, Ghosh D, Liu S,
1044 Ramos P et al. 2018. A toolbox of immunoprecipitation-grade monoclonal antibodies to
1045 human transcription factors. *Nat Methods* doi:10.1038/nmeth.4632.
- 1046 Wang J, Zhuang J, Iyer S, Lin X, Whitfield TW, Greven MC, Pierce BG, Dong X, Kundaje A,
1047 Cheng Y et al. 2012. Sequence features and chromatin structure around the genomic
1048 regions bound by 119 human transcription factors. *Genome Res* **22**: 1798-1812.
- 1049 Wardle FC, Tan H. 2015. A ChIP on the shoulder? Chromatin immunoprecipitation and
1050 validation strategies for ChIP antibodies. *F1000Res* **4**: 235.
- 1051 Weirauch MT, Yang A, Albu M, Cote AG, Montenegro-Montero A, Drewe P, Najafabadi HS,
1052 Lambert SA, Mann I, Cook K et al. 2014. Determination and inference of eukaryotic
1053 transcription factor sequence specificity. *Cell* **158**: 1431-1443.
- 1054 Winter G, Griffiths AD, Hawkins RE, Hoogenboom HR. 1994. Making antibodies by phage
1055 display technology. *Annu Rev Immunol* **12**: 433-455.
- 1056 Workman CT, Yin Y, Corcoran DL, Ideker T, Stormo GD, Benos PV. 2005. enoLOGOS: a
1057 versatile web tool for energy normalized sequence logos. *Nucleic Acids Res* **33**: W389-
1058 392.
- 1059 Yamada N, Lai WKM, Farrell N, Pugh BF, Mahony S. 2019. Characterizing protein-DNA
1060 binding event subtypes in ChIP-exo data. *Bioinformatics* **35**: 903-913.
- 1061 Zhang Y, Liu T, Meyer CA, Eeckhoute J, Johnson DS, Bernstein BE, Nusbaum C, Myers RM,
1062 Brown M, Li W et al. 2008. Model-based analysis of ChIP-Seq (MACS). *Genome Biol* **9**:
1063 R137.
- 1064

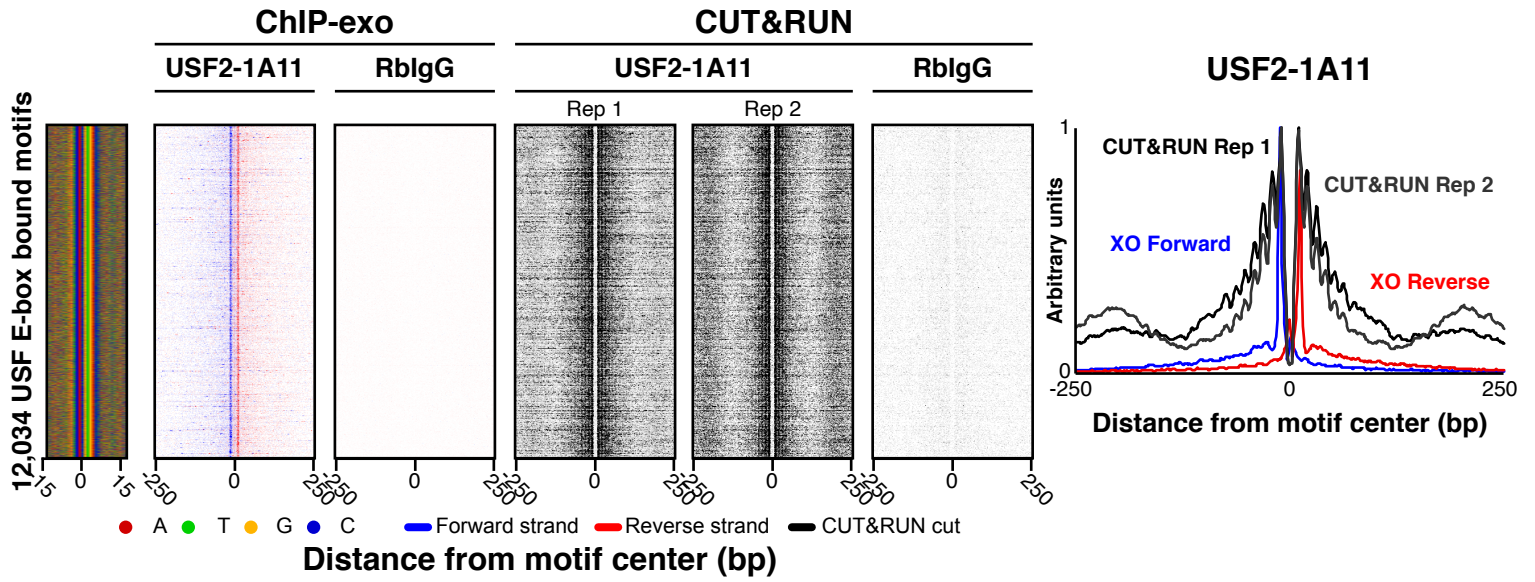








A



B

